24. Hangai M, Yamamoto M, Sakamoto A, Yoshimura N (2009) Ultrahigh-resolution versus speckle noise-reduction in spectral-domain optical coherence tomography. Opt Express 17: 4221–4235.
25. Byeon SH, Chu YK, Lee H, Lee SY, Kwon OW (2009) Foveal ganglion cell layer damage in ischemic diabetic maculopathy: correlation of optical coherence tomographic and anatomic changes. Ophthalmology 116: 1949–1959.
26. Nakano N, Hangai M, Nakanishi H, Mori S, Nukada M, et al. (2011) Macular Ganglion Cell Layer Imaging in Preperimetric Glaucoma with Speckle Noise-Reduced Spectral Domain Optical Coherence Tomography. Ophthalmology 118: 2414–2426.
27. Sandberg MA, Brockhurst RJ, Gaudio AR, Berson EL (2005) The association between visual acuity and central retinal thickness in retinitis pigmentosa. Invest Ophthalmol Vis Sci 46: 3349–3354.
28. Costa RA, Calucci D, Skaf M, Cardillo JA, Castro JC, et al. (2004) Optical coherence tomography 3: Automatic delineation of the outer neural retinal boundary and its influence on retinal thickness measurements. Invest Ophthalmol Vis Sci 45: 2399–2406.
29. Chen TC, Cense B, Miller JW, Rubin PA, Deschler DG, et al. (2006) Histologic correlation of in vivo optical coherence tomography images of the human retina. Am J Ophthalmol 141: 1165–1168.
30. Oishi A, Hata M, Shimozono M, Mandai M, Nishida A, et al. (2010) The significance of external limiting membrane status for visual acuity in age-related macular degeneration. Am J Ophthalmol 150: 27–32.
31. Murakami T, Nishijima K, Sakamoto A, Ota M, Horii T, et al. (2011) Association of pathomorphology, photoreceptor status, and retinal thickness with visual acuity in diabetic retinopathy. Am J Ophthalmol 151: 310–317.
32. Huber G, Beck SC, Grimm C, Sahaboglu-Tekgoz A, Paquet-Durand F, et al. (2009) Spectral domain optical coherence tomography in mouse models of retinal degeneration. Invest Ophthalmol Vis Sci 50: 5888–5895.
33. Kim KH, Puoris'haag M, Maguluri GN, Umino Y, Cusato K, et al. (2008) Monitoring mouse retinal degeneration with high-resolution spectral-domain optical coherence tomography. J Vis 8: 17 1–11.
34. Ruggeri M, Wehbe H, Jiao S, Gregori G, Jockovich ME, et al. (2007) In vivo three-dimensional high-resolution imaging of rodent retina with spectral-domain optical coherence tomography. Invest Ophthalmol Vis Sci 48: 1808–1814.
35. Srinivasan VJ, Ko TH, Wojtkowski M, Carvalho M, Clermont A, et al. (2006) Noninvasive volumetric imaging and morphometry of the rodent retina with high-speed, ultrahigh-resolution optical coherence tomography. Invest Ophthalmol Vis Sci 47: 5522–5528.
36. Fischer MD, Huber G, Beck SC, Tanimoto N, Muehlfriedel R, et al. (2009) Noninvasive, in vivo assessment of mouse retinal structure using optical coherence tomography. PLoS ONE 4: 1–7.
37. Nakano N, Ikeda HO, Hangai M, Muraoka Y, Toda Y, et al. (2011) Longitudinal and Simultaneous Imaging of Retinal Ganglion Cells and Inner Retinal Layers in a Mouse Model of Glaucoma Induced by N-Methyl-D-Aspartate. Invest Ophthalmol Vis Sci 52: 8754–8762.
38. Yamauchi Y, Agawa T, Tsukahara R, Kimura K, Yamakawa N, et al. (2011) Correlation between high-resolution optical coherence tomography (OCT) images and histopathology in an iodoacetic acid-induced model of retinal degeneration in rabbits. Br J Ophthalmol 95: 1161–1165.
39. Li T, Snyder WK, Olsson JE, Dryja TP (1996) Transgenic mice carrying the dominant rhodopsin mutation P347S: evidence for defective vectorial transport of rhodopsin to the outer segments. Proc Natl Acad Sci U S A 93: 14176–14181.
40. Aleman TS, Cideciyan AV, Sumaroka A, Windsor EA, Herrera W, et al. (2008) Retinal laminar architecture in human retinitis pigmentosa caused by Rhodopsin gene mutations. Invest Ophthalmol Vis Sci 49: 1580–1590.
41. Milam AH, Li ZY, Fariss RN (1998) Histopathology of the human retina in retinitis pigmentosa. Prog Retin Eye Res 17: 175–205.
42. Humayun MS, Prince M, de Juan E, Jr., Barron Y, Moskowitz M, et al. (1999) Morphometric analysis of the extramacular retina from postmortem eyes with retinitis pigmentosa. Invest Ophthalmol Vis Sci 40: 143–148.
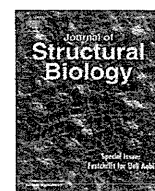
Rescue of growth defects of yeast *cdc48* mutants by pathogenic IBMPFD-VCPs

Takahiro Takata[a], Yoko Kimura[b,*], Yohei Ohnuma[a], Junko Kawawaki[b], Yukie Kakiyama[b], Keiji Tanaka[b], Akira Kakizuka[a,*]

[a] Laboratory of Functional Biology, Kyoto University Graduate School of Biostudies, Kyoto 606-8501, Japan
[b] Laboratory of Protein Metabolism, Tokyo Metropolitan Institute of Medical Science, Setagaya-ku, Tokyo 156-8506, Japan

ARTICLE INFO

ABSTRACT

VCP/p97/Cdc48 is a hexameric ring-shaped AAA ATPase that participates in a wide variety of cellular functions. VCP is a very abundant protein in essentially all types of cells and is highly conserved among eukaryotes. To date, 19 different single amino acid-substitutions in VCP have been reported to cause IBMPFD (inclusion body myopathy associated with Paget disease of bone and frontotemporal dementia), an autosomal dominant inherited human disease. Moreover, several similar single amino acid substitutions have been proposed to associate with a rare subclass of familial ALS. The mechanisms by which these mutations contribute to the pathogenesis are unclear. To elucidate potential functional differences between wild-type and pathogenic VCPs, we expressed both VCPs in yeast *cdc48* mutants. We observed that all tested pathogenic VCPs suppressed the temperature-sensitive phenotype of *cdc48* mutants more efficiently than wild-type VCP. In addition, pathogenic VCPs, but not wild-type VCP, were able to rescue a lethal *cdc48* disruption. In yeast, pathogenic VCPs, but not wild-type VCP, formed apparent cytoplasmic foci, and these foci were transported to budding sites by the Myo2/actin-mediated transport machinery. The foci formation of pathogenic VCPs appeared to be associated with their suppression of the temperature-sensitive phenotype of *cdc48* mutants. These results support the idea that the pathogenic VCP mutations create dominant gain-of-functions rather than a simple loss of functional VCP. Their unique properties in yeast could provide a convenient drug-screening system for the treatment of these diseases.

© 2012 Elsevier Inc. All rights reserved.

1. Introduction

VCP, a member of the AAA (<u>A</u>TPase <u>a</u>ssociated with diverse cellular <u>a</u>ctivities) family, is one of the most abundant and ubiquitous intracellular proteins (Jentsch and Rumpf, 2007; Stolz et al., 2011; Yamanaka et al., 2011). VCP participates in diverse cellular activities, including ubiquitin–proteasome-mediated protein degradation, endoplasmic reticulum (ER)-associated degradation (ERAD), and ER and Golgi membrane fusions. Recent studies revealed that VCP also functions in autophagy and endolysosomal sorting (Ju and Weihl, 2010; Ritz et al., 2011). To perform such diverse functions, VCP appears to differentially utilize its cofactors, which amounts, so far, to about 30 proteins (Madsen et al., 2009; Yeung et al., 2008). In addition, many amino acid residues in VCP are post-translationally modified throughout the protein via oxidation,

phosphorylation, and acetylation to regulate the function of VCP (Koike et al., 2010; Mori-Konya et al., 2009; Noguchi et al., 2005).

In addition to its various cellular roles, VCP was identified as a binding protein of the Machado-Joseph disease (MJD) protein with expanded polyglutamines (Hirabayashi et al., 2001). Subsequently, by genetic screening using *Drosophila* polyglutamine disease models, the *Drosophila* homologue of VCP, *ter94*, was identified as a modifier of expanded polyglutamine-induced eye degeneration (Higashiyama et al., 2002). In addition, VCP was found to co-localize with abnormal protein aggregates or ubiquitin-positive inclusion bodies in patient-derived neurons representative of several neurodegenerative disorders such as MJD, Huntington disease, Parkinson disease, or motor neuron diseases such as ALS (Hirabayashi et al., 2001; Ishigaki et al., 2004; Mizuno et al., 2003), suggesting that VCP is widely involved in different neurodegenerative diseases (Kakizuka, 2008).

The idea has been further supported by the discovery of missense mutations in the human *VCP* gene from patients suffering from IBMPFD (Inclusion body myopathy associated with Paget's disease of bone (PDB) and frontotemporal dementia (FTD)), a rare, complex, late-onset, and ultimately lethal disorder with autosomal dominant inheritance (OMIM 167320) (Kimonis et al., 2000; Watts

---

et al., 2004). To date, 19 different single missense mutations have been reported from IBMPFD patients (I27V, R93C, R95C/G, P137L, R155C/H/P/S/L, G157R, R159H/C, R191Q, L198W, A232E, T262A, N387H, A439S) (Ju and Weihl, 2010). In addition, four missense mutations (R155H, R191Q, R159G, D592N) in VCP were recently proposed to cause familial ALS with autosomal dominant inheritance (Johnson et al., 2010).

It has been reported that pathogenic VCPs cause various cellular defects, including disruption of ERAD (Weihl et al., 2006), impairment of aggresome formation (Ju et al., 2008), defective autophagy (Ju et al., 2009), and impaired endolysosomal sorting (Ritz et al., 2011). In cultured cells, pathogenic VCP showed altered binding abilities for cofactor(s) and ubiquitin (Fernandez-Saiz and Buchberger, 2010; Manno et al., 2010). In addition, biochemical studies revealed that pathogenic VCP adopted nucleotide-dependent altered conformations and had an increased ATPase activity compared to wild-type VCP (Halawani et al., 2009; Manno et al., 2010; Tang et al., 2010; Fernandez-Saiz and Buchberger, 2010). Several lines of evidence implicate the involvement of TDP-43 in the pathogenesis of IBMPFD in neurons (Ritson et al., 2010; Weihl et al., 2008). However, detailed molecular mechanisms underlying IBMPFD still remain largely unknown.

The yeast Saccharomyces cerevisiae provides a useful experimental system for elucidating molecular mechanisms in biological processes, due to the ease of genetic manipulations. Since many functions are conserved between yeast Cdc48 and mammalian VCP, we expressed human wild-type and pathogenic VCPs in yeast Cdc48 mutant strains, and characterized their induced phenotypes.

2. Materials and methods

2.1. Yeast strains

A list of yeast strains used in this study is provided in Sup. Table 1. The cdc48-1 strain (Y255) was created by mating DBY2030 (cdc48-1) with W303 twice (Moir et al., 1982), and the cdc48-3 strain in a W303 background (Y202) was described previously (Kimura et al., 2009). W303 ADE+(Y1043) was obtained by transforming a PCR-amplified DNA fragment containing ADE2 with 300 bp of flanking regions from both upstream and downstream of ADE2. Gene deletions for Δbni1, Δdoa10, Δpre9, Δshe4, Δufd2, Δsmy1, and Δbni1 were made with the PCR-based method using pYM1 (Janke et al., 2004; Knop et al., 1999). Gene deletion for Δbnr1 was achieved using FA6a-natNT2. Carboxyl-terminal tagging with 9xmyc for Myo2 and with 6xHA for Ufd1 or Shp1 were performed using pYM18 and pYM16, respectively. For the disruption of CDC48, first, an XhoI fragment carrying HIS3 was excised from a plasmid and inserted into the SalI site of CDC48 (nt −434 to +2585) in BSII. Then the resultant plasmid was linearized and transformed into W303 diploid cells.

2.2. Antibodies

The affinity-purified rabbit polyclonal anti-VCP and rabbit polyclonal anti-Cdc48p antibodies were developed previously (Hirabayashi et al., 2001; Noguchi et al., 2005). The following antibodies used in this study were purchased: mouse monoclonal anti-actin (Chemicon); mouse monoclonal anti-GFP for Western blot (Roche) or for immunostaining (Invitrogen); rabbit polyclonal anti-GFP (Molecular Probes); mouse monoclonal anti-HA (Roche); mouse monoclonal anti-c-myc for immunoprecipitation (9E10, Santa-Cruz); rabbit polyclonal anti-c-myc for immunostaining (CM100, Gramsch Laboratories); mouse monoclonal anti-yeast PGK antibody (Molecular Probes, Eugene, OR); Alexa Fluor 488 goat anti-mouse IgG and Alexa Fluor 594 goat anti-rabbit IgG (Molecu-

lar Probes); sheep polyclonal anti-mouse IgG-HRP and donkey anti-rabbit IgG-HRP (GE Healthcare).

2.3. Plasmids

A list of plasmids used in this study is provided in Sup. Table 2. The VCP expression plasmids (pRS316UPD-VCP or pRS316GPD-pathogenic VCP), in which VCP or pathogenic VCP are under the GPD promoter in pRS316, were created as follows. First, a BamHI and EcoRI fragment with the GPD promoter was inserted into the BamHI and EcoRI sites of pRS316 to create 316-GPD. Then BamHI and NotI fragments of VCP or pathogenic VCPs from pBS II KS(+) VCPs were inserted into the BamHI and NotI sites of 316-GPD (Mori-Konya et al., 2009). The VCP-EGFP plasmids were created by ligating BglII-NotI fragments from pEGFP-N-VCP with 316-GPD. For the plasmids expressing VCPs under the control of the CDC48 promoter, the CDC48 promoter region from −434 to −1 was amplified by PCR using genomic DNA as a template with the following primers: (AATTGTCGACCAGCCCAAGAAACGGACTTCGA TAAGTTGG, AATTGGATCCGATTTGTATATCTGTCTTGTAGTTGAGC-CA). The PCR fragment was then cut with SalI and BamHI, and ligated with the BamHI–SalI vector region of pRS316GPD-VCP or pRS316GPD-pathogenic VCPs. The plasmid expressing CPY-GFP was a kind gift from Y. Saeki. To create TRP1-based vectors, pRS314 was used instead of pRS316. Initially, protein expression of VCP[R95G] was undetectable, probably due to the codon usage of GGC for glycine. We changed the GGC to GGT, and could observe the protein expression of VCP[R95G] in yeast.

2.4. Growth assay of yeasts

Yeast cell densities were adjusted to OD600 = 1.0, and diluted serially by 10-fold dilutions. Each diluted sample was spotted on the plates. Cells were incubated for 3 days at the indicated temperatures.

2.5. Immunoblotting

For Fig. 1D and Sup. Fig. 4B, whole-cell extracts for Western blotting were prepared as described previously (Kushnirov, 2000), and for other experiments, as described previously (Kimura et al., 2001).

To measure the level of CPY*-GFP, cells were grown to mid-log phase at 30 °C, and treated with 50 μg/ml of cycloheximide. Cells were further incubated at 30 °C, and harvested at the indicated times. Western blotting analysis was performed using anti-GFP and anti-PGK.

2.6. FACS analysis

Cells were treated with 15 μg/ml nocodazole for 120 min, washed twice with water, and suspended in medium. Then the temperature was shifted. At the indicated times, cells were fixed in 70% ethanol, resuspended in a Tris–citrate buffer (180 mM Tris–HCl (pH 7.5), 180 mM NaCl, 70 mM $MgCl_2$, 50 mM sodium citrate), briefly sonicated, and digested with 0.25 mg/ml RNase in the same buffer for 1 h at 50 °C. DNA was stained with 50 μg/ml propidium iodide, and 50,000 cells from each sample were scanned with a FACScan flow cytometer (BD Biosciences) as described previously FL2H = 37(Threshold).

2.7. Microscopic analysis of EGFP-fusion proteins

For the observation of EGFP-fusion proteins in Figs. 4, 5B–E, 6B and C, 7A–C, cells were imaged at room temperature using an OLY-

PUS BX51 microscope equipped with OLMPUS UIS2 uPlan SApo 40X/0.90 ∞/0.11-0.23/FN26.5.

2.8. Rhodamine–phalloidin staining

Cells at early log phase (1–3 × 10⁶/ml, 10 ml) were fixed by adding one-tenth volume of 37% formaldehyde and incubating at 25 °C for 30 min. Cells were harvested, washed twice with PBS by centrifugation at 3000 rpm for 2 min, and suspended in 200 µl of PBS, and sonicated briefly. Half of the cells were treated with 5 U of rhodamine–phalloidin (Molecular Probes) for 10 min, washed with PBS three times, and suspended in 50 µl of PBS. Cells were imaged at room temperature using a confocal microscope (LSM510; Carl Zeiss) equipped with Plan-Apochromat 100× oil objective lenses. Images were acquired as z sections of 0.37 µm. Images were processed in the LSM image browser, and brightness and contrast were adjusted using Adobe Photoshop CS4.

2.9. Immunostaining analysis

Yeast cells in early log-phase were fixed with 3.7% formaldehyde for 1 h, and washed twice with buffer B (20 mM potassium phosphate pH 7.4, 1.2 M sorbitol). Cells were treated with Zymolyase (final 0.5 mg/ml) in buffer B plus 0.17% of 2-mercaptoethanol, and incubated at 30 °C for 10 min. Cells were centrifuged at 5000 rpm for 1 min, then washed three times with buffer B. Swelling buffer (20 mM MES pH 6.0, 150 mM potassium acetate, 5 mM magnesium acetate, 750 mM sorbitol) was added and cells were incubated at room temperature for 20 min. Cells were mounted on a cover slip for 5 min, then treated with methanol for 5 min and acetone for 5 min. Mount blocking solution (2% skim milk and 0.1% Tween20 in PBS) was added to the cover glass for 30 min, and anti-GFP and anti-myc antibodies in blocking buffer

were incubated at 4 °C overnight. Secondary antibodies (Alexa488 anti-rabbit IgG, Alexa594 anti-mouse IgG) were incubated at room temperature for 2 h and washed twice with PBS containing BSA (final 0.01 mg/ml). Cells were imaged using a confocal microscope (LSM510; Carl Zeiss) equipped with Plan-Apochromat 100× oil objective lens. Images were acquired as z sections of 0.37 µm.

2.10. Time-lapse imaging

Cell morphologies and GFP signals were recorded every 10 min using an inverted fluorescence microscope (Axiovert 200M; Carl Zeiss). Image analysis and processing were performed via the Zeiss AxioVision 4.5 software.

2.11. Statistical analysis

Each experiment was conducted at least three times with consistent results. The gel or blot representative of each experiment is presented in this study. The statistical significance was analyzed using Student's t test against the corresponding values of the wild type.

3. Results

3.1. Rescue of temperature-sensitive growth of cdc48 mutants by the expression of pathogenic VCPs but not wild-type VCP

To elucidate potential disease-related functions of pathogenic VCPs, we expressed wild-type VCP (wtVCP) and pathogenic VCPs (R93C, R95G, R155C, R155H, R155P, R159H, R191Q, and A232E) in yeast S. cerevisiae. Since porcine VCP, which is 70% identical to yeast Cdc48 at the amino acid level, has been shown not to be able to complement a cdc48 null mutation (Madeo et al., 1997), we ex-
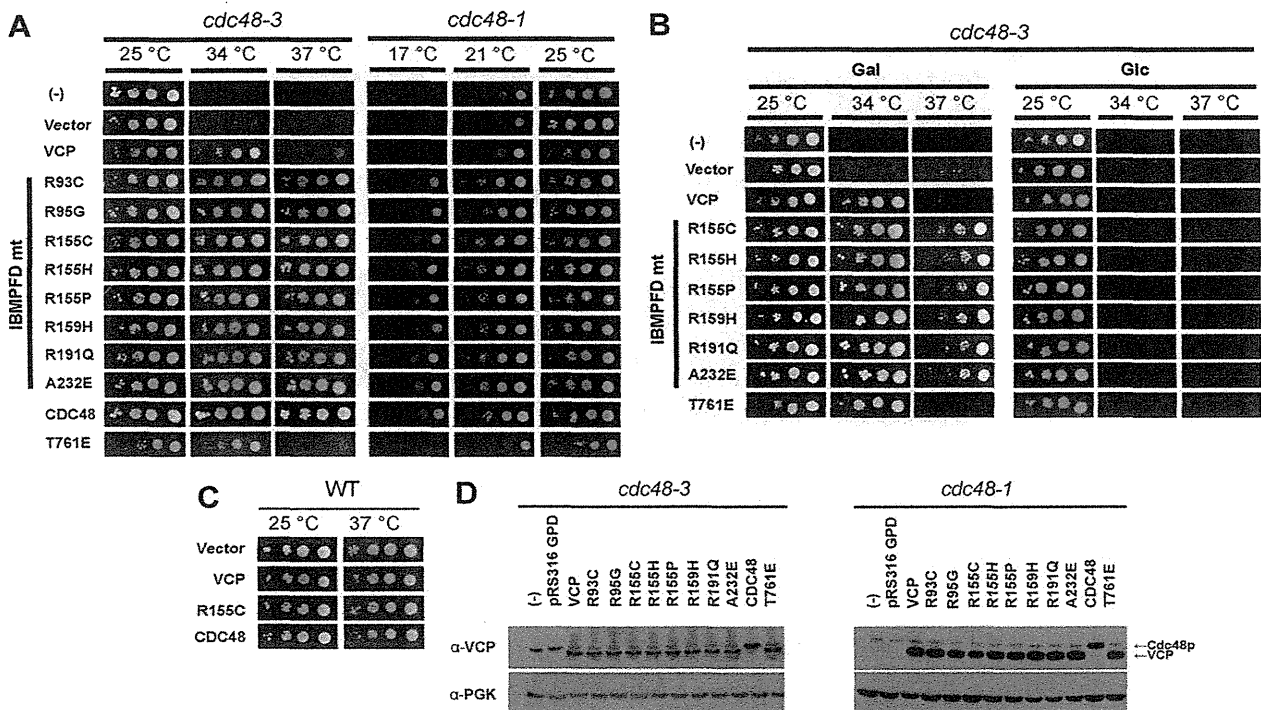

Fig.1. Effective suppression of temperature-sensitivities of cdc48-3 and cdc48-1 by pathogenic VCPs. (A) Effects of the expression of various VCPs under the control of the GPD promoter on the growth of cdc48-3 and cdc48-1. The cdc48 mutant cells with or without exogenously expressed VCPs or Cdc48 were diluted and spotted on SD uracil (−) plates, and grown at the indicated temperatures for 3 days. (B) Effects of the expression of various VCPs under the GAL promoter on the growth of cdc48-3. Cells were spotted on SGal uracil (−) plates, and grown at the indicated temperatures for 3 days. (C) Effects of the expression of VCP, VCP[R155C] or CDC48 under the GPD promoter on the growth of wild type cells. (D) Expression levels of various VCPs and Cdc48 proteins in cdc48-3 and cdc48-1. Cells grown at 25 °C were analyzed by Western blot using an anti-VCP antibody. PGK serves as a control for loading. Note that yeast Cdc48 cross-reacted with anti-VCP antibody as shown.

pressed these VCPs in high-temperature-sensitive (ts) cdc48-3 and cold-sensitive (cs) cdc48-1 mutants under the control of the constitutive GPD promoter. The amino acid sequences of wild-type human, rat, and mouse VCPs are 100% identical and are 70% identical to yeast Cdc48. The expression of wtVCP partially suppressed the ts growth of cdc48-3 but not the cs growth of cdc48-1 (Fig. 1A). Surprisingly, we observed that eight pathogenic VCPs tested here were all able to rescue the temperature-sensitive growth of both cdc48-3 and cdc48-1 mutants (Fig. 1A). Similar phenotypes were also observed by expressing VCPs under the control of the galactose-inducible GAL promoter (Fig. 1B). In these experiments, all of the GAL promoter-induced mutant VCPs (R155C, R155H, R155P, R159H, R191Q, and A232E), efficiently rescued the ts phenotype of the cdc48-3 mutant both at 34 °C and 37 °C, whereas wtVCP rescued only at 34 °C. Expression of pathogenic VCP[R155C] in wild-type cells did not affect the growth phenotypes both at 25 and 37 °C (Fig. 1C). We confirmed that the expression levels of all VCPs including wtVCP were mostly equivalent (Fig. 1D). Thus, the observed difference between wtVCP and the pathogenic VCPs appeared not to be due to the levels of proteins, but rather due to their intrinsic activities. Since these pathogenic VCPs have increased ATPase activities (Halawani et al., 2009; Manno et al., 2010), we examined whether VCP[T761E], a mutant with the highest ATPase activity known (Mori-Konya et al., 2009), had an even better ability to suppress the ts phenotypes than the pathogenic VCPs (Fig. 1A and B). However, VCP[T761E] behaved more like wtVCP and was not able to suppress the ts phenotypes as effectively as the pathogenic VCPs, suggesting that the increased ATPase activities of the pathogenic VCPs were not related to the suppression of the temperature-sensitive cdc48 mutant phenotypes.

In addition, pathogenic VCPs (R155C or A232E) were expressed under the CDC48 promoter (nt −434 to −1, with respect to the start of transcription), resulting in expression levels that were only about to 1/10–1/15 relative to proteins expressed under the GPD promoter. Nevertheless, they still rescued the temperature-sensitivity of cdc48-3, though the suppression was less effective than in cells expressing the mutant protein under the GPD promoter (Sup. Fig. 1).

We then examined whether the expression of pathogenic VCP (via the GPD promoter) could rescue the cell cycle defects of cdc48 mutations (Sup. Fig. 2A). To differentiate between wtVCP and pathogenic VCP in liquid culture more clearly, the temperatures of 32.5 °C and 35.5 °C were chosen, since not only wtVCP but also pathogenic VCP did not seem to have any effect on cell cycle progression of cdc48-3 mutants in liquid culture at 37 °C. Cells were first synchronized with nocodazole, released and shifted to 32.5 °C and 35.5 °C, then analyzed by FACS analysis based on DNA contents. At 32.5 °C, we found that the cell cycle arrest observed in cdc48-3 was rectified by the expression of both wtVCP and VCP[R155C]. By contrast, at 35.5 °C, the arrest was rescued by the expression of VCP[R155C] but not wtVCP (Sup. Fig. 2A).

3.2. Rescue of the lethal cdc48 null mutation by pathogenic, but not wild-type, VCP

The result that pathogenic VCPs but not wtVCP allowed cdc48 temperature-sensitive mutants to grow at restrictive temperatures led us to examine whether pathogenic VCPs were also able to rescue a cdc48 null mutation. For this purpose, we introduced a URA3-based plasmid expressing wtVCP or pathogenic VCPs under the GPD promoter into a diploid Δcdc48 heterozygote strain (CDC48/cdc48::HIS3). After these diploids sporulated, they were dissected. As Cdc48 is essential, usually only two colonies arose from the Δcdc48 heterozygote. In segregants of the diploids expressing pathogenic VCP [R93C, R95G, R155C, R191Q, or A232E], but not wtVCP, we often obtained small colonies in addition to two colonies of a regular size (Fig. 2A). All of the small colonies were
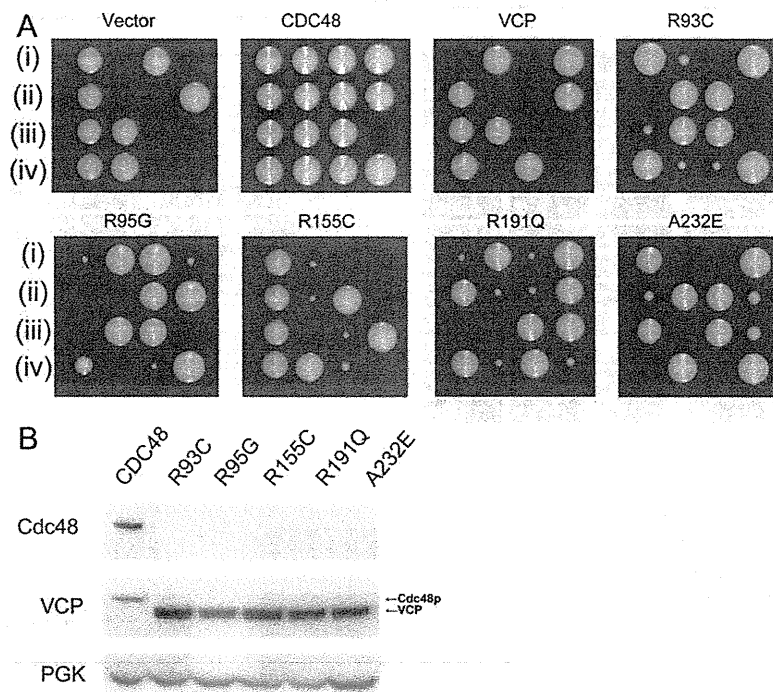

Fig.2. Complementation of the lethal cdc48 null mutant by pathogenic VCPs. (A) Diploid strain (Δcdc48::HIS3/CDC48) transformed with or without a URA3-containing expression plasmid for Cdc48, wtVCP, VCP[R93C], VCP[R95G], VCP[R155C], VCP[R191Q], or VCP[A232E], was dissected after sporulation. In these experiments, Cdc48 was expressed under its cognate promoter, and wild-type and pathogenic VCPs were expressed under the GPD promoter. In each tetrad analysis, four sets of segregants are shown in (i)–(iv) (each tetrad is displayed horizontally). (B) Expression levels of VCP and Cdc48 proteins were examined for his+, ura+ segregants obtained from each tetrad. PGK serves as a loading control.

his+, ura+ cells, indicating that the *cdc48::HIS3* cells were viable when the pathogenic VCP-expressing plasmid was transmitted to the *cdc48::HIS3* segregant. Similar results were obtained using a Δ*cdc48::kanR/CDC48* strain, another heterozygote (data not shown). By Western blot analysis of these his+ ura+ cells, we confirmed that pathogenic VCP but not Cdc48 was expressed (Fig. 2B). In addition, DNA sequence analysis of plasmids recovered from these cells confirmed the presence of the respective pathogenic VCP mutations (data not shown). In segregants of the diploids expressing wtVCP, we observed only two colonies at most from 40 different tetrad analyses.

To exclude the possibility that plasmid transmission through meiosis was defective in the cells expressing wtVCP, we performed a plasmid swapping assay using 5-FOA, a compound that kills ura+ cells. A *cdc48* null mutant that was rescued by a *URA3* plasmid expressing Cdc48 was transformed with a *TRP1* plasmid expressing wtVCP, pathogenic VCPs or Cdc48. After culturing on uracil-containing plates to let cells drop the *URA3* plasmid, cells were streaked on 5-FOA plates. Only *cdc48* null mutants that could survive without the *URA3* plasmid grow on the 5-FOA plates. As expected, cells expressing pathogenic VCPs or Cdc48 grew but not wtVCP were able to grow on 5-FOA plates (Sup. Fig. 3).

Since the expression of pathogenic VCPs under the control of the *CDC48* promoter rescued the temperature-sensitivity of *cdc48-3* to a certain extent (Fig. S1), we investigated whether the same pathogenic VCPs driven by the CDC48 promoter could also rescue a null mutation of *cdc48*. We found that the lethality of the *cdc48* null mutation was not rescued (data not shown). Thus, these results indicate that a sufficient amount of pathogenic VCPs, but not wtVCP, was able to rescue the *cdc48* null mutation.

3.3. Partial rescue of Cdc48 activities by expression of wild-type VCP and pathogenic VCPs

We then examined whether pathogenic VCPs were able to rescue another characteristic defect of the Cdc48 mutation, namely the impaired ability to degrade CPY*, a Cdc48-specific substrate (Ye et al., 2001). In the *cdc48-3* mutant, degradation of CPY*-GFP, a GFP-tagged CPY*, was delayed, and expression of Cdc48 rescued the defect (Fig. 3). We found that the expression of wtVCP partially rescued the CPY*-GFP degradation defect in *cdc48-3* cells. Expression of VCP[R155C] and VCP[A232E] also partially rescued the degradation defect in *cdc48-3* cells, to a similar extent as wtVCP, but were not as robust as for Cdc48. These results suggest that the differing capacities of the wild-type and pathogenic VCPs to rescue the growth defects of *cdc48* mutants are not attributable to differences in the ability to degrade Cdc48 substrates.

3.4. Foci formation of pathogenic VCPs

To further differentiate between wtVCP and pathogenic VCPs, we examined the localization of these VCPs. To observe their localization, we expressed VCPs fused with EGFP. We first verified that EGFP-fused VCPs functioned similarly to non-tagged VCPs. EGFP-fused pathogenic VCPs suppressed the temperature sensitivity of *cdc48-3* much more efficiently than wtVCP-EGFP (Sup. Fig. 4). Moreover, EGFP-fused pathogenic VCPs (R155C, R191Q, A232E) as well as CDC48-EGFP, but not wtVCP-EGFP, rescued a null mutation of *cdc48* (Sup. Fig. 4). In *cdc48-3* cells, Cdc48-EGFP and wtVCP-EGFP showed a diffuse localization throughout the cells (Fig. 4A). Interestingly, VCP[R155C]-EGFP exhibited a small
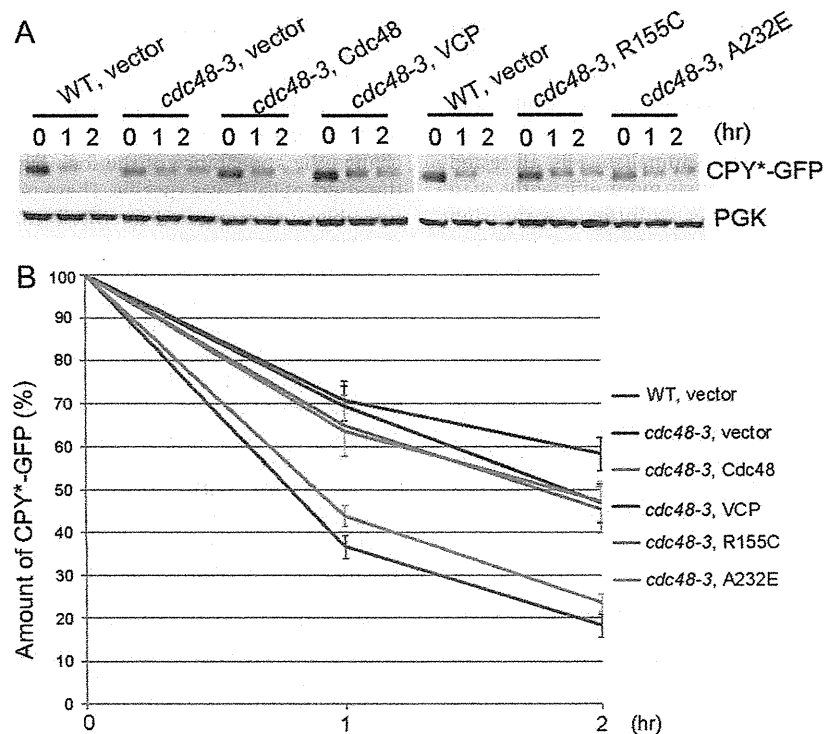

Fig.3. Degradation of CPY*-GFP. (A) Wild-type and *cdc48-3* cells with or without an expression plasmid for CPY*-GFP, with or without plasmids expressing Cdc48, wtVCP, VCP[R155C], or VCP[A232E] were grown at 30 °C to mid-log phase. They were treated with cycloheximide (50 µg/ml), and harvested at the indicated times. The expression of CPY*-GFP was examined by Western blot using an anti-GFP antibody. (B) Quantification of the amount of CPY*GFP in (A). Protein levels were quantified from the bands shown in (A). Data are mean ± SE values of three independent experiments. In each experiment, the amount of CPY*-GFP at time 0 was defined as 100%.
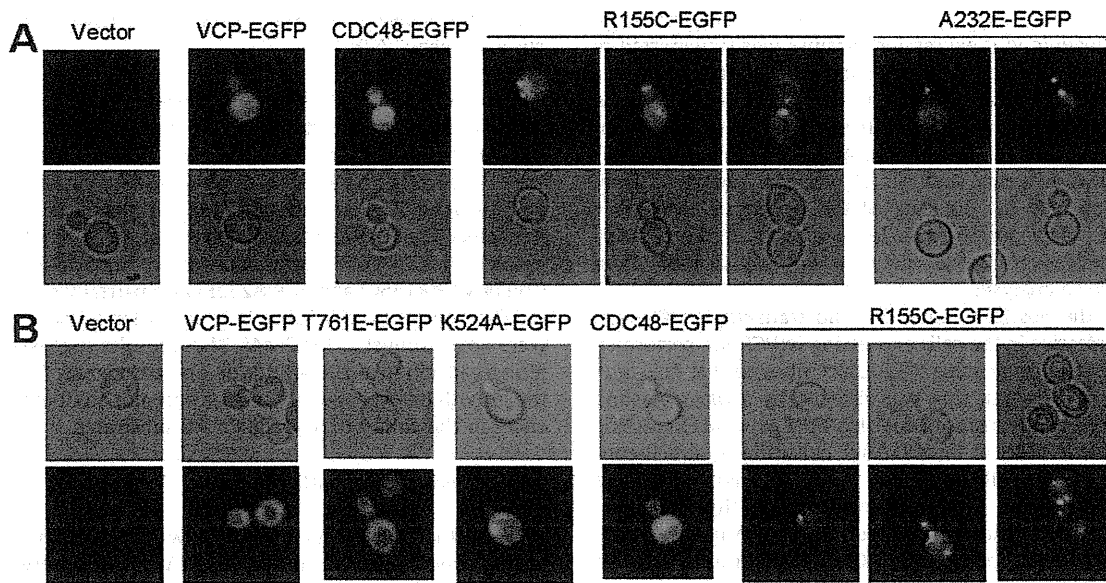
Fig.4. Foci formation of pathogenic VCPs. (A) Foci formation in *cdc48-3* cells expressing VCP[R155C]-EGFP or VCP[A232E]-EGFP, but not in *cdc48-3* cells expressing wtVCP- or Cdc48-EGFP. The *cdc48-3* cells with the indicated plasmids were cultured to an early log phase and examined by fluorescence microscopy. (B) Foci formation in wild-type cells expressing VCP[R155C]-EGFP, but not in cells expressing wtVCP-, VCP[T761E]-, VCP[K524A]-, or Cdc48-EGFP.

number of strong GFP foci within a diffuse background of GFP fluorescence (Fig. 4A). These foci were not localized within the nucleus, when counterstained by Hoechst (data not shown). We observed quite similar GFP-foci in VCP[A232E]-EGFP-expressing cells (Fig. 4A). Moreover, the GFP foci were not uniquely observed in *cdc48-3* cells: we observed similar VCP[R155C]-EGFP foci in wild-type yeast cells (Fig. 4B). Immuno-staining using an anti-VCP antibody yielded a similar result: VCP[R155C] formed foci, but wtVCP did not (Sup. Fig. 5). Furthermore, neither VCP[K524A]-EGFP nor VCP[T761E]-EGFP formed foci (Fig. 4B). These results indicate that focus formation was associated with pathogenic VCP mutations, but was not directly linked to different ATPase activities of VCPs.

It has been shown that these pathogenic VCPs adopt different ATP-dependent conformations from wtVCP (Halawani et al., 2009; Tang et al., 2010). Moreover, in mammalian cells, all tested pathogenic VCPs formed aggregates much more efficiently than wtVCP, when they were expressed either with the co-expression of polyglutamines or with the treatment of proteasome inhibitors (Ju et al., 2008; Manno et al., 2010). In addition, Cdc48 was reported to be included in an aggresome (Wang et al., 2009). Thus, it is easy to speculate that these foci may be simple aggregates incorporating the pathogenic VCPs. However, considering that pathogenic VCPs are better able to suppress the defects of *cdc48* mutants, these foci may be functional complexes, or otherwise beneficial to the *cdc48* mutants. Indeed, as both nocodazole and benomyl treatment did not affect the localization and appearance of the foci, it is not likely that the foci are aggresomes (Fig. 5B and C, and data not shown). Rather, we noticed that the GFP foci were often localized at the buds (Fig. 4).

3.5. Involvement of actin cables in foci formation of pathogenic VCPs

We speculated that there might be a specific mechanism to generate VCP[R155C]-EGFP foci at buds. It is known that in budding yeasts many organelles and vesicles are conveyed toward buds by polarized transport utilizing actin cables as rails (Pruyne et al., 2004b). We therefore examined whether actin was involved in the localization of the foci at buds. First, we examined whether VCP[R155C]-EGFP foci were co-localized on actin by phalloidin

staining. Indeed, VCP[R155C]-EGFP foci in buds were partially co-localized on the phalloidin-positive structures (Fig. 5A). Next, we examined whether actin cables were required for the specific localization of foci at buds by treating cells with Latrunculin B (LatB), which inhibits actin polymerization by sequestering actin monomers (Ayscough et al., 1997; Irazoqui et al., 2005). After LatB treatment, we observed that the VCP[R155C]-EGFP foci disappeared; instead, multiple small punctate structures appeared throughout the cell (Fig. 5B and C). When LatB was washed out from the medium, the VCP[R155C]-EGFP foci were reformed, and the foci moved to buds (Fig. 5D and E). By time-lapse analysis, we observed that the VCP[R155C]-EGFP-containing small punctae started to fuse to make foci and then the foci moved to buds (Sup. Fig. 6). Treatment with nocodazole, MG132, tunicamycin, or heat shock did not change the appearance of the foci (Fig. 5B and C), indicating that the effect of LatB was specific. These results demonstrated that actin cables were required for the formation of the foci as well as their transport to buds.

We investigated the involvement of actin cables in more detail. Actin cables are filamentous structures that emanate from a site of polarized growth in budding yeast (Fig. 6A) (Pruyne et al., 2004b). In budding yeast, the assembly of actin cables is controlled by the formins Bni1 and Bnr1. Bni1 nucleates actin cables that originate in the bud, whereas Bnr1 polymerizes actin cables at the bud neck (Pruyne et al., 2004a). We therefore examined whether VCP[R155C]-EGFP foci formed in Δ*bni1* and Δ*bnr1* cells. Similar to the results with LatB-treated cells, GFP fluorescence of VCP[R155C]-EGFP showed multiple punctae in Δ*bni1* cells and Δ*bnr1* cells (Fig. 6B and C). The alteration of GFP patterns was much clearer in Δ*bni1* cells than in Δ*bnr1* cells. In contrast, GFP fluorescence remained diffuse in Δ*bni1* and Δ*bnr1* cells expressing wtVCP-EGFP or Cdc48-EGFP (Fig. 6B and C). VCP[R155C]-EGFP foci formation was tested in other mutant cells, and was not impaired in a Pre9 (a proteasome subunit) mutant, a Doa10 (ubiquitin ligase in ERAD) mutant, or a Ufd2 (ubiquitin chain assembly factor) mutant, suggesting that UPS machinery was not involved in the foci formation (Fig. 6C).

We next examined whether the VCP[R155C]-EGFP foci formation at buds was related to its function in the suppression of
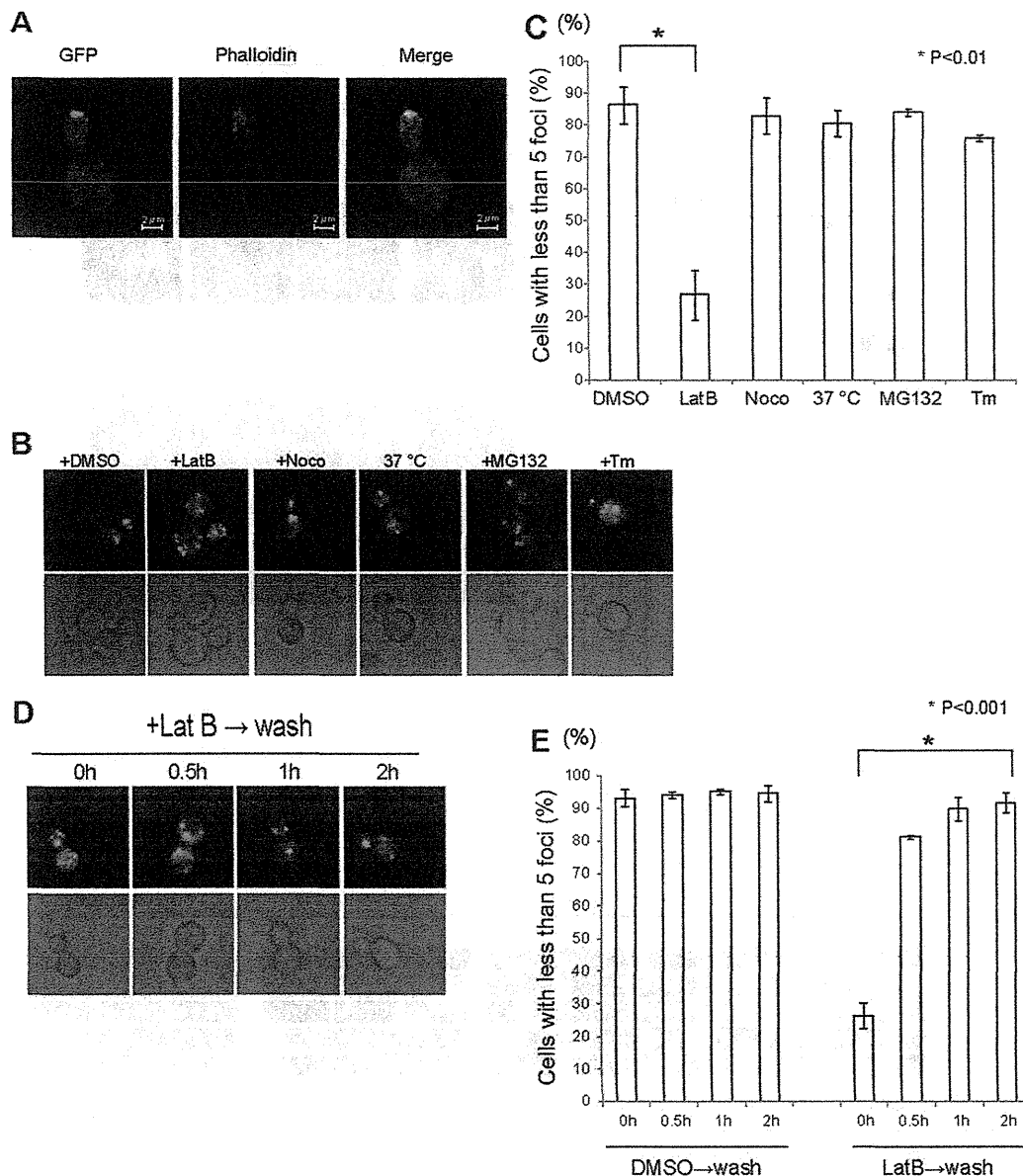
Fig.5. Involvement of actin cables in the formation and localization of VCP[R155C] foci at buds. (A) Phalloidin staining. Wild-type cells (Y1043) expressing VCP[R155C]-EGFP in early log phase were fixed, stained with rhodamine–phalloidin, and analyzed by confocal microscopy. (B) Latrunculin B, nocodazole, heat shock, MG132 and tunicamycin treatment. Wild-type cells expressing VCP[R155C]-EGFP were treated with Latrunculin B (25 μg/ml) for 2 h, nocodazole (15 μg/ml) for 2 h, a heat shock of 37 °C for 2 h, MG132 (200 μM) for 4 h, or with tunicamycin (2 μg/ml) for 4 h at 25 °C, and the cells were examined by fluorescence microscopy. (C) Quantification of (B). Cells containing less than 5 bright GFP foci throughout the cell were counted among a total of 100 cells in (B), and mean values of three experiments are shown. SD are shown as bars. Note that a decrease of cells with foci ($n < 5$) indicates a reciprocal increase of cells with numerous punctae ($5 \leqslant n$). (D) Re-formation of VCP[R155C]-EGFP foci after washing out of Latrunculin B. Wild-type cells expressing VCP[R155C]-EGFP were treated with Latrunculin B (25 μg/ml in DMSO) for 2 h, washed twice with 1% DMSO, incubated in medium with 1% DMSO, and examined at the indicated times by fluorescence microscopy. (E) Quantification of (D). Results are shown, as described in (C). Note that an increase of cells with foci ($n < 5$) indicates reciprocal decrease of cells with only punctae ($5 \leqslant n$).

cdc48 temperature-sensitivity. For this purpose, we created the double-mutant strains cdc48-3 Δbni1 and cdc48-3 Δbnr1, expressed VCP[R155C]-EGFP in these mutants, and grew them at restrictive temperatures. The suppression activity of VCP[R155C]-EGFP on the growth defects was partially lost in both cdc48-3 Δbnr1 and cdc48-3 Δbni1 cells at the restrictive temperature of 37 °C but not at 34 °C (Fig. 6D). The Δbni1 single mutant cells grew well at either 25 °C or 37 °C, and the growth of Δbni1 cells was not affected by the expression of wtVCP, VCP[R155C], or CDC48 (Sup. Fig. 7). These results support the idea that focus formation of VCP[R155C]-EGFP at buds was required for suppression of the cdc48 ts mutation.

3.6. Involvement of Myo2 in foci formation of pathogenic VCPs

Of the five myosins in yeast, it is notable that Class V myosins (Myo2, and Myo4) are motor proteins or cages that transport their cargos toward the plus ends of actin filaments. The cargos include vacuoles, small organelles, secretary vesicles, and components of TGN (Trans Golgi Network) (Trybus, 2008). While Myo4 mediates the transport of mRNA and movement of ER tubules, Myo2 plays a major role in the transport of secretory vesicles, vacuoles, and segregation of membrane-bound organelles (Matsui, 2003). Therefore, we next examined the formation and the movement of VCP[R155C]-EGFP foci in two temperature-sensitive myo2 mutant
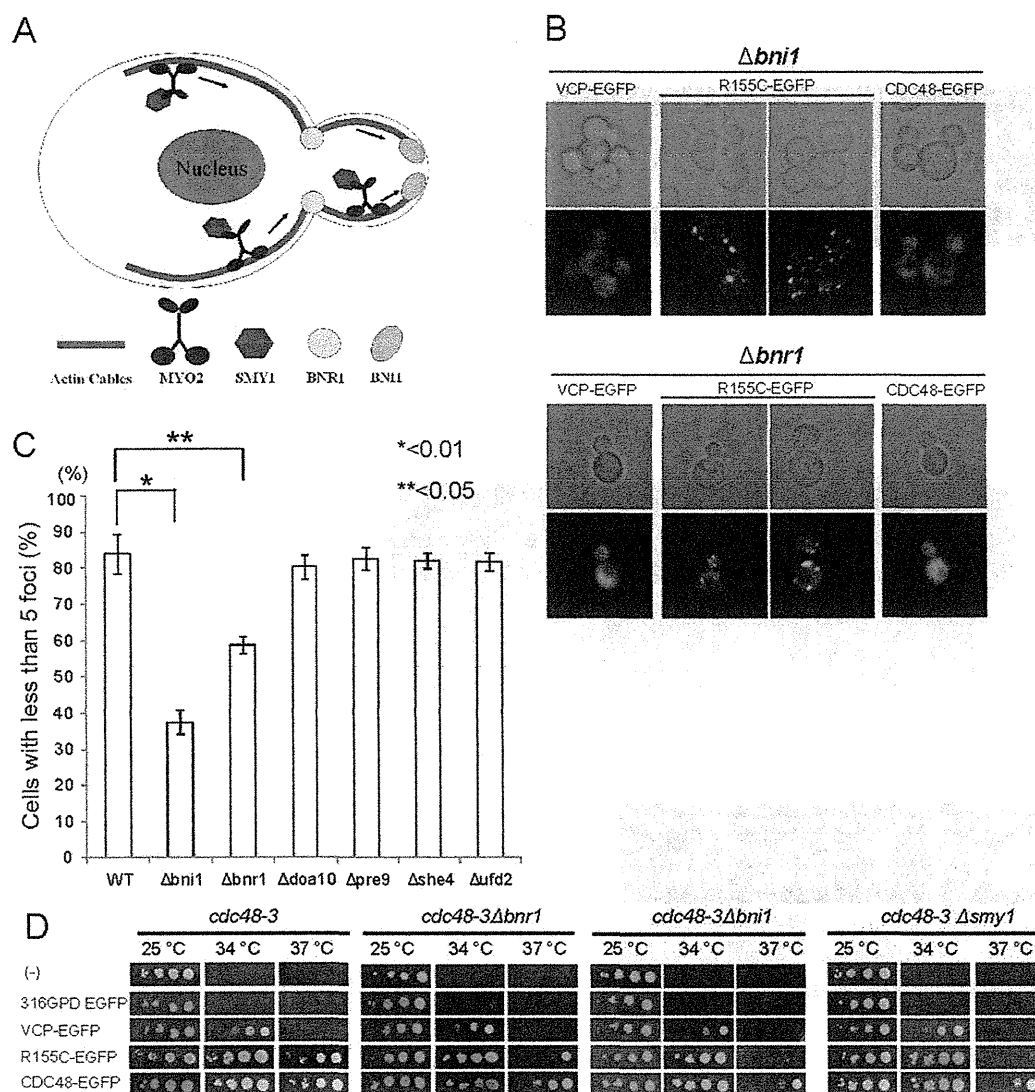
Fig.6. Effects of BNI1 and BNR1. (A) schematic drawing of the actin-mediated transport machinery of a budding cell. (B) GFP fluorescence images of wtVCP-, VCP[R155C]-, or CDC48-EGFP in Δbni1 and Δbnr1 mutants. (C) Quantification of foci formations in various mutants, as indicated. Results are shown, as described in Fig. 5C. Note that a decrease of cells with foci ($n < 5$) indicates a reciprocal increase of cells with numerous punctae ($5 \leqslant n$). (D) Growth of cdc48-3, cdc48-3Δbnr1, cdc48-3Δbni1, cdc48-3Δsmy1 expressing EGFP, wtVCP-, VCP[R155C]-, or Cdc48-EGFP at the indicated temperatures.

backgrounds, myo2-66 and myo2-20. In myo2-66 cells, myo2 is defective in its actin binding domain, and in myo2-20 cells its tail domain is defective in cargo binding (Johnston et al., 1991; Schott et al., 1999). In both mutants, VCP[R155C]-EGFP fluorescence appeared as multiple small punctate structures, which were similar to those observed in Δbni1 and Δbnr1 cells, as well as LatB-treated cells (Fig. 7A and B). Frequencies of foci localization in buds also significantly decreased in both of the myo2 mutants (Fig. 7A and C). Moreover, in a strain with a deletion of Smy1, a kinesin-related protein that interacts with Myo2 (Beningo et al., 2000), small multiple punctae were also observed (Fig. 7A–C). Consistent with the formation of small punctae, a partial loss of suppression by VCP[R155C]-EGFP was observed in cdc48-3 Δsmy1 cells at the restrictive temperature, 37 °C (Fig. 6D). By contrast, VCP[R155C]-EGFP foci formation was retained in a myo1 mutant and a Δshe4 mutant whose function is required for Myo4, Myo3, and Myo5, thus confirming the specific involvement of Myo2 (Figs. 6C and 7A–C). Attempts to make double mutants of myo2-66 cdc48-3 and myo2-20 cdc48-3 were unsuccessful (data not shown).

In addition, we observed the co-localization, albeit partial, of Myo2 and VCP[R155C]-EGFP in wild-type cells (Fig. 7D), which further supports the idea that Myo2 is responsible for the transport of VCP[R155C]-EGFP itself or a VCP[R155C]-EGFP-containing cargo(s). Interestingly, VCP[R155C]-EGFP did not co-localize with actin in the myo2-66 mutant, though the localization of actin did not appear to change, as compared to wild-type cells (Fig. 7E). These results suggest that the interaction between VCP[R155C]-EGFP foci and actin was not direct; rather, the interaction was mediated by Myo2.

We next attempted to demonstrate physical interactions between VCP[R155C]-EGFP and Myo2 by co-immunoprecipitation analysis (Sup. Fig. 8). Under conditions in which VCP[R155C]-EGFP interacted with Ufd1-6HA and Shp1-6HA efficiently, we could not clearly detect interactions between VCP[R155C]-EGFP and Myo2. Thus, although VCP[R155C]-EGFP and Myo2 were apparently co-localized, their interaction might not be direct; there might be a protein or proteins that link VCP[R155C] and Myo2.
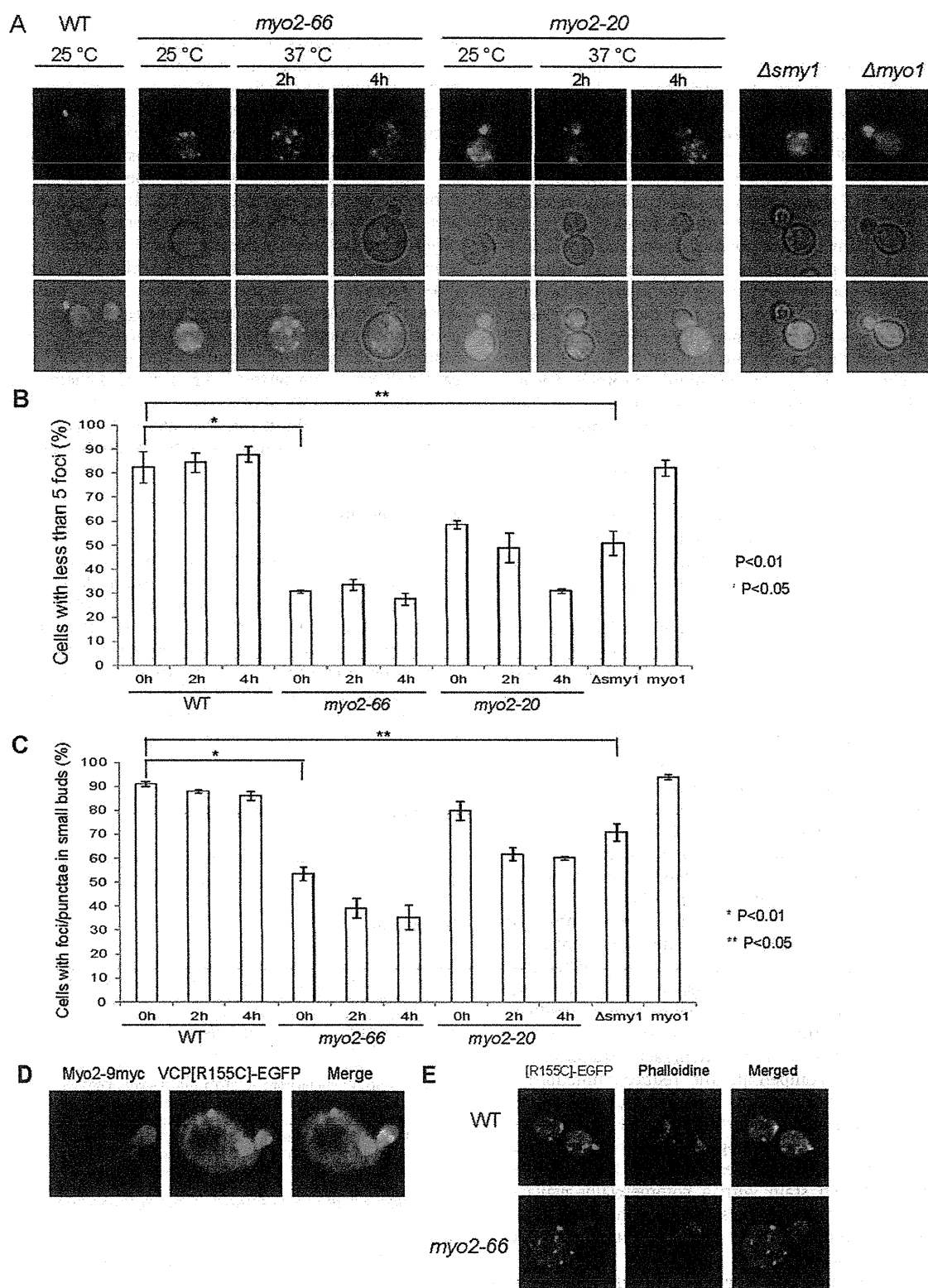
Fig.7. Myo2-dependent VCP[R155C] foci formation and its transport to buds. (A) GFP fluorescence images of VCP[R155C]-EGFP. Wild-type, myo2-66, myo2-20, Δsmy1, and myo1 cells expressing VCP[R155C]-EGFP were grown at 25 °C. In myo2-66 and myo2-20 mutants, cells were shifted to 37 °C for 2 and 4 h. Upper panels, GFP fluorescence; middle panels, phase contrast; lower panels, merged. (B) Quantification of cells with foci throughout the cell in (A). Results are shown, as described in Fig. 5C. Note that a decrease of cells with foci (n < 5) indicates a reciprocal increase of cells with numerous punctae (5 ⩽ n). (C) Quantification of cells with foci/punctae in buds in (A). Cells with a bud whose size was less than half of its mother cell were scored for whether the bud had foci/punctae or not. Note that a decrease of cells with foci/punctae in buds indicates a reciprocal increase of cells without foci/punctae in buds. (D) Co-localization of Myo2-9myc and VCP[R155C]-EGFP expressed in wild-type. Cells grown at 25 °C were stained with anti-myc and anti-GFP antibodies and analyzed by confocal microscopy. (E) GFP fluorescence and phalloidin-stained images of wild-type and myo2-66 cells expressing VCP[R155C]-EGFP, analyzed by confocal microscopy.

4. Discussion

In this study, we showed that mutations observed in pathogenic IBMPFD VCPs, which are eventually detrimental to humans, are beneficial to yeast cdc48 mutants. This suggests that these pathogenic VCPs have some critical functions that cdc48 mutants need for growth, which wtVCP does not provide. From this point of view, the various amino acid substitutions observed in IBMPFD might commonly change VCP functionally to more closely resemble Cdc48. This idea would fit well with the observations that all tested pathogenic VCPs similarly rescued not only the ts growth of cdc48-1 and cdc48-3 but also the lethality of the cdc48 null mutation. However, this might not be the case, for the following reasons: first, all of the pathogenic mutations we tested occur on residues conserved between yeast and human (R93, R95, R155, R159, R191 and A232). Thus, these mutations reduced the overall amino acid homology between the yeast and human proteins. Second, regarding the function of substrate degradation in yeast, both pathogenic VCPs and wtVCP behaved very similarly, but less efficiently than yeast Cdc48. Third, and most importantly, the pathogenic VCPs required the Myo2-actin transport system to allow cdc48 mutants to grow, but in wild-type yeast, the endogenous Cdc48 protein apparently does not need the Myo2-actin transport system for growth; i.e., myo2 mutant cells, myo2-66 and myo2-20, are able to grow. These results imply that the pathogenic VCPs have acquired some new functions that wtVCP and yeast Cdc48 do not possess.

The growth arrest of cdc48-1 and cdc48-3 at restrictive temperatures occurs in G2/M phase (Moir et al., 1982), at which the most apparent change was the loss of progression of mitosis. Interestingly, the pathogenic VCPs tended to accumulate at budding sites and made clear foci, and this accumulation and foci formation appeared to be responsible for following progression of mitosis and eventual progression of the cell cycle in cdc48-1 and cdc48-3 mutants. For these phenotypes, the pathogenic VCPs required the Myo2-actin transport system. In this system, Myo2, a member of the myosin V family, functions as a cage to transport cargos (materials), necessary for progression of mitosis, along actin fibers to buds, though we were unable to detect any physical interaction between the pathogenic VCPs and Myo2. We speculate that the pathogenic VCPs, either by chance or not, acquired a binding affinity to a yet unknown cargo(s) of the Myo2 cage, and thus were transported to buds. At restrictive temperature, the functions of cdc48-1 and cdc48-3 proteins are weakened, to a level that is not enough to support mitotic progression. Even in these conditions, when high amounts of pathogenic VCPs, by themselves or as a complex, are provided to buds via the Myo2-actin transport system, they were able to compensate the reduced functions of cdc48-1 and cdc48-3 proteins. We are currently investigating whether pathogenic VCPs affect the actin-mediated transport system in mammalian cells. Since pathogenic VCP, transfected into mammalian cells forms foci in the presence of MG132, we tested whether these foci would stain with a commercially-available anti-myosin V, but this antibody was not able to detect them. Therefore, as yet, we do not have clear evidence that similar structures exist in mammalian cells.

Interestingly, structural analysis revealed that many of the mutated residues are located at the interface between the N-terminus domain (N domain) and the first ATPase domain (D1 domain) (Tang et al., 2010; Fernandez-Saiz and Buchberger, 2010). Furthermore, it was proposed that altered rhythms of N domain movement occur in the pathogenic VCPs, which are presumably caused by the altered ATP hydrolysis cycle of the mutants (Tang et al., 2010). These reports further support the idea that common structural changes may occur in pathogenic VCPs, and these changes may be related to their ability to form foci in yeast as well as the complementation of cdc48 mutants.

Since VCP is an abundant protein and interacts with many proteins, a pathogenic VCP likely affects many cell functions in mammalian cells, whether or not they are related to IBMPFD or ALS pathologies. Molecular promiscuity notwithstanding, IBMPFD and ALS caused by pathogenic VCPs are autosomal dominant disorders, and thus the pathogenic VCPs are expected to acquire common dominant functions over the wtVCP. In this study, we showed that all tested pathogenic VCPs could rescue the growth of cdc48-1 and cdc48-3 mutants, even in the presence of endogenous mutated proteins. Although it is currently not clear that this dominant phenotype represents a certain disease-related disorder, further elucidation of the mechanism underlying this phenotype may contribute to the understanding of the pathology of IBMPFD and ALS. Moreover, the yeast expressing pathogenic VCPs would provide easy drug screening systems; e.g., screening chemical compounds for suppression of the temperature-sensitivity, for viability, or for foci formation would be possible, and may also contribute to the development of new drug candidates for the treatment of IBMPFD and ALS.

Appendix A. Supplementary data

Supplementary data associated with this article can be found, in the online version, at http://dx.doi.org/10.1016/j.jsb.2012.06.005.

References

Ayscough, K.R., Stryker, J., Pokala, N., Sanders, M., Crews, P., Drubin, D.G., 1997. High rates of actin filament turnover in budding yeast and roles for actin in establishment and maintenance of cell polarity revealed using the actin inhibitor latrunculin-A. J. Cell Biol. 137, 399–416.
Beningo, K.A., Lillie, S.H., Brown, S.S., 2000. The yeast kinesin-related protein Smy1p exerts its effects on the class V myosin Myo2p via a physical interaction. Mol. Biol. Cell 11, 691–702.
Fernandez-Saiz, V., Buchberger, A., 2010. Imbalances in p97 co-factor interactions in human proteinopathy. EMBO Rep. 11, 479–485.
Halawani, D., LeBlanc, A.C., Rouiller, I., Michnick, S.W., Servant, M.J., Latterich, M., 2009. Hereditary inclusion body myopathy-linked p97/VCP mutations in the NH2 domain and the D1 ring modulate p97/VCP ATPase activity and D2 ring conformation. Mol. Cell. Biol. 29, 4484–4494.
Higashiyama, H., Hirose, F., Yamaguchi, M., Inoue, Y.H., Fujikake, N., Matsukage, A., Kakizuka, A., 2002. Identification of ter94, Drosophila VCP, as a modulator of polyglutamine-induced neurodegeneration. Cell Death Differ. 9, 264–273.
Hirabayashi, M., Inoue, K., Tanaka, K., Nakadate, K., Ohsawa, Y., Kamei, Y., Popiel, A.H., Sinohara, A., Iwamatsu, A., Kimura, Y., Uchiyama, Y., Hori, S., Kakizuka, A., 2001. VCP/p97 in abnormal protein aggregates, cytoplasmic vacuoles, and cell death, phenotypes relevant to neurodegeneration. Cell Death Differ. 8, 977–984.
Irazoqui, J.E., Howell, A.S., Theesfeld, C.L., Lew, D.J., 2005. Opposing roles for actin in Cdc42p polarization. Mol. Biol. Cell 16, 1296–1304.
Ishigaki, S., Hishikawa, N., Niwa, J., Iemura, S., Natsume, T., Hori, S., Kakizuka, A., Tanaka, K., Sobue, G., 2004. Physical and functional interaction between Dorfin and Valosin-containing protein that are colocalized in ubiquitylated inclusions in neurodegenerative disorders. J. Biol. Chem. 279, 51376–51385.
Janke, C., Magiera, M.M., Rathfelder, N., Taxis, C., Reber, S., Maekawa, H., Moreno-Borchart, A., Doenges, G., Schwob, E., Schiebel, E., Knop, M., 2004. A versatile toolbox for PCR-based tagging of yeast genes: new fluorescent proteins, more markers and promoter substitution cassettes. Yeast 21, 947–962.

Jentsch, S., Rumpf, S., 2007. Cdc48 (p97): a "molecular gearbox" in the ubiquitin pathway? Trends Biochem. Sci. 32, 6–11.

Johnson, J.O., Mandrioli, J., Benatar, M., Abramzon, Y., Van Deerlin, V.M., Trojanowski, J.Q., Gibbs, J.R., Brunetti, M., Gronka, S., Wuu, J., Ding, J., McCluskey, L., Martinez-Lage, M., Falcone, D., Hernandez, D.G., Arepalli, S., Chong, S., Schymick, J.C., Rothstein, J., Landi, F., Wang, Y.D., Calvo, A., Mora, G., Sabatelli, M., Monsurro, M.R., Battistini, S., Salvi, F., Spataro, R., Sola, P., Borghero, G., Galassi, G., Scholz, S.W., Taylor, J.P., Restagno, G., Chio, A., Traynor, B.J., 2010. Exome sequencing reveals VCP mutations as a cause of familial ALS. Neuron 68, 857–864.

Johnston, G.C., Prendergast, J.A., Singer, R.A., 1991. The Saccharomyces cerevisiae MYO2 gene encodes an essential myosin for vectorial transport of vesicles. J. Cell. Biol. 113, 539–551.

Ju, J.S., Weihl, C.C., 2010. Inclusion body myopathy, Paget's disease of the bone and fronto-temporal dementia: a disorder of autophagy. Hum. Mol. Genet. 19, R38–R45.

Ju, J.S., Miller, S.E., Hanson, P.I., Weihl, C.C., 2008. Impaired protein aggregate handling and clearance underlie the pathogenesis of p97/VCP-associated disease. J. Biol. Chem. 283, 30289–30299.

Ju, J.S., Fuentealba, R.A., Miller, S.E., Jackson, E., Piwnica-Worms, D., Baloh, R.H., Weihl, C.C., 2009. Valosin-containing protein (VCP) is required for autophagy and is disrupted in VCP disease. J. Cell Biol. 187, 875–888.

Kakizuka, A., 2008. Roles of VCP in human neurodegenerative disorders. Biochem. Soc. Trans. 36, 105–108.

Kimonis, V.E., Kovach, M.J., Waggoner, B., Leal, S., Salam, A., Rimer, L., Davis, K., Khardori, R., Gelber, D., 2000. Clinical and molecular studies in a unique family with autosomal dominant limb-girdle muscular dystrophy and Paget disease of bone. Genet. Med. 2, 232–241.

Kimura, Y., Koitabashi, S., Kakizuka, A., Fujita, T., 2001. Initial process of polyglutamine aggregate formation in vivo. Genes Cells 6, 887–897.

Kimura, Y., Yashiroda, H., Kudo, T., Koitabashi, S., Murata, S., Kakizuka, A., Tanaka, K., 2009. An inhibitor of a deubiquitinating enzyme regulates ubiquitin homeostasis. Cell 137, 549–559.

Knop, M., Siegers, K., Pereira, G., Zachariae, W., Winsor, B., Nasmyth, K., Schiebel, E., 1999. Epitope tagging of yeast genes using a PCR-based strategy: more tags and improved practical routines. Yeast 15, 963–972.

Koike, M., Fukushi, J., Ichinohe, Y., Higashimae, N., Fujishiro, M., Sasaki, C., Yamaguchi, M., Uchihara, T., Yagishita, S., Ohizumi, H., Hori, S., Kakizuka, A., 2010. Valosin-containing protein (VCP) in novel feedback machinery between abnormal protein accumulation and transcriptional suppression. J. Biol. Chem. 285, 21736–21749.

Kushnirov, V.V., 2000. Rapid and reliable protein extraction from yeast. Yeast 16, 857–860.

Madeo, F., Schlauer, J., Frohlich, K.U., 1997. Identification of the regions of porcine VCP preventing its function in Saccharomyces cerevisiae. Gene 204, 145–151.

Madsen, L., Seeger, M., Semple, C.A., Hartmann-Petersen, R., 2009. New ATPase regulators – p97 goes to the PUB. Int. J. Biochem. Cell Biol. 41, 2380–2388.

Manno, A., Noguchi, M., Fukushi, J., Motohashi, Y., Kakizuka, A., 2010. Enhanced ATPase activities as a primary defect of mutant valosin-containing proteins that cause inclusion body myopathy associated with Paget disease of bone and frontotemporal dementia. Genes Cells 15, 911–922.

Matsui, Y., 2003. Polarized distribution of intracellular components by class V myosins in Saccharomyces cerevisiae. Int. Rev. Cytol. 229, 1–42.

Mizuno, Y., Hori, S., Kakizuka, A., Okamoto, K., 2003. Vacuole-creating protein in neurodegenerative diseases in humans. Neurosci. Lett. 343, 77–80.

Moir, D., Stewart, S.E., Osmond, B.C., Botstein, D., 1982. Cold-sensitive cell-division-cycle mutants of yeast: isolation, properties, and pseudoreversion studies. Genetics 100, 547–563.

Mori-Konya, C., Kato, N., Maeda, R., Yasuda, K., Higashimae, N., Noguchi, M., Koike, M., Kimura, Y., Ohizumi, H., Hori, S., Kakizuka, A., 2009. P97/valosin-containing protein (VCP) is highly modulated by phosphorylation and acetylation. Genes Cells 14, 483–497.

Noguchi, M., Takata, T., Kimura, Y., Manno, A., Murakami, K., Koike, M., Ohizumi, H., Hori, S., Kakizuka, A., 2005. ATPase activity of p97/valosin-containing protein is regulated by oxidative modification of the evolutionarily conserved cysteine 522 residue in Walker A motif. J. Biol. Chem. 280, 41332–41341.

Pruyne, D., Gao, L., Bi, E., Bretscher, A., 2004a. Stable and dynamic axes of polarity use distinct formin isoforms in budding yeast. Mol. Biol. Cell 15, 4971–4989.

Pruyne, D., Legesse-Miller, A., Gao, L., Dong, Y., Bretscher, A., 2004b. Mechanisms of polarized growth and organelle segregation in yeast. Annu. Rev. Cell Dev. Biol. 20, 559–591.

Ritson, G.P., Custer, S.K., Freibaum, B.D., Guinto, J.B., Geffel, D., Moore, J., Tang, W., Winton, M.J., Neumann, M., Trojanowski, J.Q., Lee, V.M., Forman, M.S., Taylor, J.P., 2010. TDP-43 mediates degeneration in a novel Drosophila model of disease caused by mutations in VCP/p97. J. Neurosci. 30, 7729–7739.

Ritz, D., Vuk, M., Kirchner, P., Bug, M., Schutz, S., Hayer, A., Bremer, S., Lusk, C., Baloh, R.H., Lee, H., Glatter, T., Gstaiger, M., Aebersold, R., Weihl, C.C., Meyer, H., 2011. Endolysosomal sorting of ubiquitylated caveolin-1 is regulated by VCP and UBXD1 and impaired by VCP disease mutations. Nat. Cell Biol. 13, 1116–1123.

Schott, D., Ho, J., Pruyne, D., Bretscher, A., 1999. The COOH-terminal domain of Myo2p, a yeast myosin V, has a direct role in secretory vesicle targeting. J. Cell. Biol. 147, 791–808.

Stolz, A., Hilt, W., Buchberger, A., Wolf, D.H., 2011. Cdc48: a power machine in protein degradation. Trends Biochem. Sci. 36, 515–523.

Tang, W.K., Li, D., Li, C.C., Esser, L., Dai, R., Guo, L., Xia, D., 2010. A novel ATP-dependent conformation in p97 N-D1 fragment revealed by crystal structures of disease-related mutants. EMBO J. 29, 2217–2229.

Trybus, K.M., 2008. Myosin V from head to tail. Cell. Mol. Life Sci. 65, 1378–1389.

Wang, Y., Meriin, A.B., Zaarur, N., Romanova, N.V., Chernoff, Y.O., Costello, C.E., Sherman, M.Y., 2009. Abnormal proteins can form aggresome in yeast: aggresome-targeting signals and components of the machinery. FASEB J. 23, 451–463.

Watts, G.D., Wymer, J., Kovach, M.J., Mehta, S.G., Mumm, S., Darvish, D., Pestronk, A., Whyte, M.P., Kimonis, V.E., 2004. Inclusion body myopathy associated with Paget disease of bone and frontotemporal dementia is caused by mutant valosin-containing protein. Nat. Genet. 36, 377–381.

Weihl, C.C., Dalal, S., Pestronk, A., Hanson, P.I., 2006. Inclusion body myopathy-associated mutations in p97/VCP impair endoplasmic reticulum-associated degradation. Hum. Mol. Genet. 15, 189–199.

Weihl, C.C., Temiz, P., Miller, S.E., Watts, G., Smith, C., Forman, M., Hanson, P.I., Kimonis, V., Pestronk, A., 2008. TDP-43 accumulation in inclusion body myopathy muscle suggests a common pathogenic mechanism with frontotemporal dementia. J. Neurol. Neurosurg. Psychiatry 79, 1186–1189.

Yamanaka, K., Sasagawa, Y., Ogura, T., 2011. Recent advances in p97/VCP/Cdc48 cellular functions. Biochim. Biophys. Acta 1823, 130–137.

Ye, Y., Meyer, H.H., Rapoport, T.A., 2001. The AAA ATPase Cdc48/p97 and its partners transport proteins from the ER into the cytosol. Nature 414, 652–656.

Yeung, H.O., Kloppsteck, P., Niwa, H., Isaacson, R.L., Matthews, S., Zhang, X., Freemont, P.S., 2008. Insights into adaptor binding to the AAA protein p97. Biochem. Soc. Trans. 36, 62–67.

In Vitro Modeling of Paraxial Mesodermal Progenitors Derived from Induced Pluripotent Stem Cells

Hidetoshi Sakurai[1,2]*, Yasuko Sakaguchi[1,3], Emi Shoji[1], Tokiko Nishino[2], Izumi Maki[2], Hiroshi Sakai[1], Kazunori Hanaoka[4], Akira Kakizuka[3], Atsuko Sehara-Fujisawa[1]

1 Department of Growth Regulation, Institute for Frontier Medical Sciences, Kyoto University, Kyoto, Japan, 2 Department of Clinical Application, Center for iPS Cell Research and Application, Kyoto University, Kyoto, Japan, 3 Laboratory of Functional Biology, Graduate School of Biostudies, Kyoto University, Kyoto, Japan, 4 Molecular Embryology, Department of Bioscience, School of Science, Kitasato University, Kanagawa, Japan

Abstract

Induced pluripotent stem (iPS) cells are generated from adult somatic cells by transduction of defined factors. Given their unlimited proliferation and differentiation potential, iPS cells represent promising sources for cell therapy and tools for research and drug discovery. However, systems for the directional differentiation of iPS cells toward paraxial mesodermal lineages have not been reported. In the present study, we established a protocol for the differentiation of mouse iPS cells into paraxial mesodermal lineages in serum-free culture. The protocol was dependent on Activin signaling in addition to BMP and Wnt signaling which were previously shown to be effective for mouse ES cell differentiation. Independently of the cell origin, the number of transgenes, or the type of vectors used to generate iPS cells, the use of serum-free monolayer culture stimulated with a combination of BMP4, Activin A, and LiCl enabled preferential promotion of mouse iPS cells to a PDGFR-α^+/Flk-1$^-$ population, which represents a paraxial mesodermal lineage. The mouse iPS cell-derived paraxial mesodermal cells exhibited differentiation potential into osteogenic, chondrogenic, and myogenic cells both in vitro and in vivo and contributed to muscle regeneration. Moreover, purification of the PDGFR-α^+/KDR$^-$ population after differentiation allowed enrichment of human iPS cell populations with paraxial mesodermal characteristics. The resultant PDGFR-α^+/KDR$^-$ population derived from human iPS cells specifically exhibited osteogenic, chondrogenic, and myogenic differentiation potential in vitro, implying generation of paraxial mesodermal progenitors similar to mouse iPS cell-derived progenitors. These findings highlight the potential of protocols based on the serum-free, stepwise induction and purification of paraxial mesodermal cell lineages for use in stem cell therapies to treat diseased bone, cartilage, and muscle.

Introduction

Embryonic stem (ES) cells have been investigated both as an experimental tool for developmental biology and as a source of cell-based therapies due to their potential for self-renewal and differentiation into all cell lineages. Novel ES cell-like pluripotent stem cells, termed induced pluripotent stem (iPS) cells, have been generated from mouse [1] and human [2,3] somatic cells by the introduction of 4 transcription factors. These iPS cells have opened the gateway for cell transplantation-based regenerative medicine by overcoming the ethical argument against human ES cells [4]. The original technology to generate iPS cells depended on the stable integration of 4 transgenes. However, the use of non-integrative vectors for gene transfer [5] or replacement of the c-Myc oncogene with other safer genes such as L-Myc [6] or Glis-1 [7] permits generation of iPS cells that lack transgenes or oncogenes. Such technical advancements reduce the risk of tumorigenesis that results from reactivation of c-Myc transgenes. However, there is still a risk of teratoma formation, derived from

residual undifferentiated cell populations after transplantation of differentiated iPS cells. Thus, efficient differentiation of iPS cells into the progenitor cells of interest and their maximal purification is required before transplantation. Moreover, suitable differentiation markers should be used to determine the signaling mechanisms that govern pluripotent stem cell differentiation toward specific lineages, so that recombinant proteins and small molecules can be used to direct differentiation.

Previously, we employed a murine ES cell in vitro differentiation culture system to show that expression of platelet-derived growth factor receptor α (PDGFR-α) allows efficient identification of paraxial mesodermal progenitors in combination with negative selection of Flk-1 expression–a lateral mesodermal marker [8]. The expression of PDGFR-α was detected in the paraxial mesoderm and somites as well as in neural tube and future spinal cord during mouse embryogenesis [9,10]. Analysis of the in vitro fate of ES cell-derived PDGFR-α^+/Flk-1$^-$ cells demonstrated their potential to differentiate into osteocytes, chondrocytes, and skeletal

muscle cells, which are derivatives of somites [8,11]. We also showed that mouse ES cells can be directed toward the paraxial mesodermal lineage by a combination of bone morphogenetic protein (BMP) [12] and Wnt [13] signaling under chemically-defined conditions [14]. However, it is not known whether iPS cells also have the potential to give rise to paraxial mesodermal lineages by stimulating BMP and Wnt signaling cascades.

In the present study, we show that BMP4 and LiCl, which activate Wnt signaling, promote differentiation of both mouse iPS and ES cells to paraxial mesodermal lineages under serum-free conditions. However, unlike mouse ES cells, the self-renewal and differentiation of mouse iPS cells to paraxial mesodermal lineages is highly dependent on Activin A [15], which prevents apoptosis of mouse iPS cells in serum-free condition. In this serum-free differentiation system, mouse iPS cells efficiently differentiate into PDGFR-α^+/Flk-1$^-$ paraxial mesodermal progenitors and, to a lesser extent, into PDGFR-α^+/Flk-1$^+$ immature and PDGFR-α^-/Flk-1$^+$ lateral mesodermal progenitors. The iPS cell-derived paraxial mesodermal progenitors exhibit osteogenic, chondrogenic, and myogenic differentiation potential both in vitro and in vivo. Moreover, sorting of PDGFR-α-positive and KDR [16] (a human homolog of mouse Flk-1)-negative populations also allows enrichment of paraxial mesodermal progenitors in induced human iPS cells which give rise to osteogenic, chondrogenic and myogenic cells in vitro.

Results

Activin A is an Essential Factor for Paraxial Mesodermal Differentiation of Mouse iPS Cells

To establish chemically defined conditions for paraxial mesodermal differentiation in vitro, iPS cells must be cultured without feeder cells. Thus, the growth-factor requirement of mouse iPS cells during paraxial mesodermal differentiation was analyzed by performing an in vitro differentiation study with various doses of growth factors in chemically defined culture conditions. First, we assessed the effect of Activin A–a member of the transforming growth factor beta super family–during the first 3 days of differentiation (Fig. 1A). Differentiation of iPS cells without Activin A resulted in minimal proliferation/survival in the absence of feeder cells (Fig. 1B). However, the addition of Activin A dramatically enhanced cell number in a dose-dependent manner (Fig. 1B). Even low dose addition of Activin A supported efficient cell proliferation (Fig. 1C). Because we observed large amount of cell death in this serum-free condition, we assessed apoptosis at 24 hour after induction. Although, the serum-free condition caused apoptosis in more than 80% of iPS cells, addition of Activin A prevented apoptosis considerably (Fig. 1D). Previously, we have demonstrated that mouse ES cells can differentiate into paraxial mesoderm only with an addition of BMP4 in serum-free conditions [14]. Therefore, we compared the response of mouse iPS cells to Activin A with that of mouse ES cells. Surprisingly, mouse ES cells showed fewer apoptosis even in the absence of Acitivin A (Fig. S1A). Mouse ES cells showed higher expression level of endogenous Nodal [17] transcription than mouse iPS cells at 24 after induction (Fig. S1B), suggesting that mouse ES cells could survive in serum-free condition producing Nodal signaling. On the other hand, expressions of early mesoendodermal or mesodermal markers, such as Mixl1 [18], Gsc [19], T [20] and Eomes [21], on day3 were enhanced by administration of Activin A in both mouse ES cells and mouse iPS cells (Fig. S1C), suggesting that Activin-Nodal signal directed differentiation toward mesodermal cells in both types of pluripotent stem cells.

Subsequently, paraxial mesodermal differentiation was assessed by the expression of PDGFR-α [8]. The addition of 5 ng/ml Activin A resulted in an increase in the number of cells expressing PDGFR-α to over 30%, and higher doses of Activin A increased the percentage of PDGFR-α^+ cells in a dose-dependent manner (Fig. 1E).

The PDGFR-α^+ cells were sorted and the gene expression level of mesodermal markers in each PDGFR-α^+ population was analyzed by quantitative real-time RT-PCR. In Activin A-depleted conditions, there were not enough PDGFR-α^+ cells to allow evaluation of mesodermal induction by RT-PCR analysis. While all samples were PDGFR-α^+, the gene expression levels of paraxial mesodermal markers (Tbx6 [22] and Mesp2 [23]) varied with the dose of Activin A– expression was high in preparations treated with the lowest dose of Activin A and low in those treated with higher doses (Fig. 1F). In contrast, Activin A did not affect the expression level of late mesodermal markers such as the dermomyotome marker Pax3 [24] and the myotome marker Myf5 [25] (Fig. 1F). Thus, the addition of high doses of Activin A may alter the characteristics of the PDGFR-α^+ population in mouse iPS cells. Since further lower dose of Activin A than 5 ng/ml did not influence the induction of paraxial mesodermal differentiation significantly (Fig. S1D), we used 5–20 ng/ml Activin A in further experiments because of dose-dependent proliferation/survival rates of iPS cells.

BMP4 Enhances Cell Proliferation and Affects Lineage-specific Gene Expression during Mouse iPS Cell Differentiation

We subsequently assessed the effect of BMP4 during the first 3 days of differentiation under chemically defined culture conditions in the presence of Activin A (Fig. 2A). The addition of BMP4 enhanced cell number in a dose-dependent manner (Fig. 2B). While the addition of high dose of BMP4 enhanced cell proliferation (Fig.2C), the absence of BMP4 resulted in large apoptosis (Fig. 2D). These two functions of BMP4 administration cooperated to increase cell number in a dose-dependent manner.

However, the generation of the PDGFR-α^+ population was unaffected by BMP4 treatment (Fig. 2E). The expression of paraxial mesodermal markers (Tbx6 [22] and Mesp2 [23]) was high when cells were induced with a medium dose (10 ng/ml) of BMP4 (Fig. 2F). In contrast, the addition of a high dose of BMP4 reduced the expression level of myogenic mesodermal markers, Pax3 [24] and Myf5 [25] (Fig. 2F). Down-regulation of Myf5 by high-dose BMP4 administration is consistent with the evidence that BMP4 acts as an inhibitor for expression of myogenic regulatory genes Myf5 and MyoD in mouse embryogenesis [26].

Wnt Signaling Enhances Paraxial Mesodermal Differentiation of Mouse iPS Cells

The effects of growth factors involved in somitogenesis during mouse development were assessed. During the last 3 days of differentiation in chemically defined culture conditions, mouse iPS cells were cultured in the presence or absence of LiCl and Sonic hedgehog (Shh), respectively (Fig. 3A). The suitable dose of LiCl and Shh were determined by induction level of PDGFR-α^+ cells, respectively (Fig. S2A and S2B). LiCl enhances Wnt signaling by translocation of β-catenin from cytoplasm to nucleus (Fig. S2C) followed by inhibiting the activity of GSK3β [27]. The addition of both LiCl and Shh to the chemically defined medium enhanced cell number (Fig. 3B). The increase of cell number was mainly due to effects of Shh in cell proliferation (Fig. S2D), whereas the addition of LiCl inhibited apoptosis (Fig. S2E). While the addition
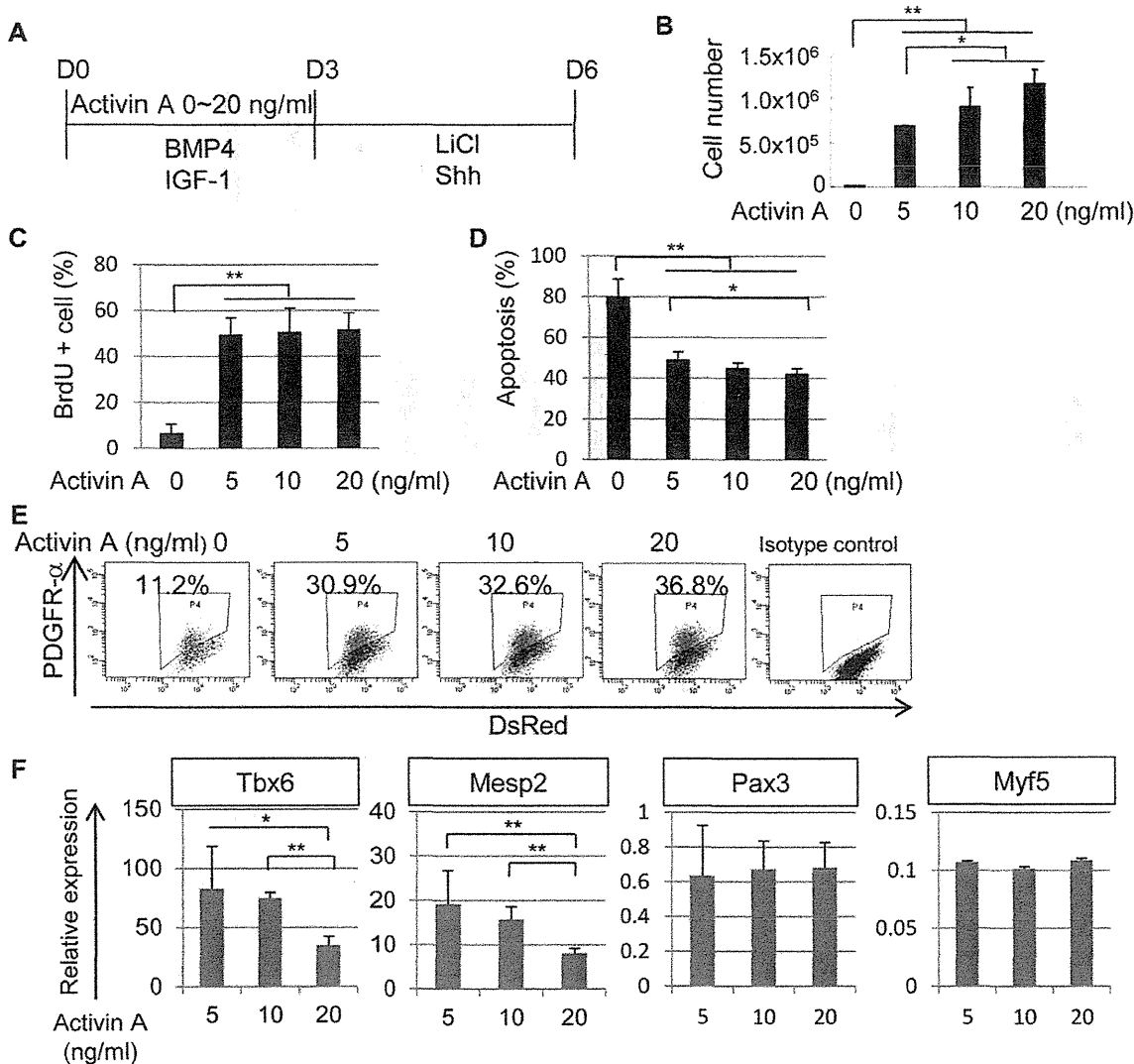
Figure 1. Effects of Activin A on paraxial mesodermal differentiation of mouse iPS cells. (A) A scheme for paraxial mesodermal differentiation of mouse iPS cells with different concentrations of Activin A from day 0 (D0) to day 3 (D3). Activin A was administrated from D0 to D3 at a concentration of 0–20 ng/ml. The cultures also contained BMP4 (10 ng/ml), IGF-1 (10 ng/ml), LiCl (5 mM), and Shh (10 ng/ml). The cells were analyzed on day 6 (D6) in (B), (E), and (F), or on day 1 (D1) in (C) and (D). (B) Total number of mouse iPS cells after differentiation with the protocol shown in (A) (n = 3). (C) Proliferation of differentiated mouse iPS cells on D1 assessed by BrdU assay (n = 3). (D) Apoptosis of differentiated mouse iPS cells on D1 assessed by a proportion of Propidium Iodide (PI) positive/AnnexinV positive cell (n = 3). (E) Dose-dependent induction of PDGFR-α by Activin A in mouse iPS cell differentiation culture. The percentage indicates the proportion of PDGFR-α⁺ cells (n = 3). (F) Gene expression profiles of PDGFR-α⁺ cells in Activin A-induced cultures (n = 3). The expression level of *Tbx6* and *Mesp2* genes was reduced in a dose-dependent manner. *p<0.05, **p<0.01 between selected two samples.
doi:10.1371/journal.pone.0047078.g001

of Shh did not influence generation of PDGFR-α⁺ cells in differentiation culture, LiCl prominently induced a PDGFR-α⁺ cell population (Fig. 3C). Moreover, the expression levels of *Tbx6* [22] were higher in the presence of LiCl, whereas the expression levels of *Mesp2* [23] and *Pax3* [24] remained unchanged under these conditions (Fig. 3D). The addition of LiCl, but not Shh, induced the expression of the myogenic mesodermal marker *Myf5* [25] (Fig. 3D). Thus, activation of Wnt signaling by LiCl promoted paraxial mesodermal differentiation of iPS cells, particularly to skeletal muscle cell lineages.

Given the aforementioned results, we optimized the culture conditions for paraxial mesodermal differentiation, as described in

the Materials and Methods. The resulting differentiation protocol was applicable to all types of iPS cells examined, including those derived from adult tail-tip fibroblast (TTF) or mouse embryonic fibroblast (MEF) cells and those made by retroviral transgenesis with 3 or 4 factors or plasmid vectors (Fig. 3E). PDGFR-α⁺ cells are distinguishable by their piled-up morphology like somite in the differentiation culture (Fig. S3). Although PDGFR-α⁺ cells can be divided into 2 distinct populations by the co-expression of Flk-1, up to 90% of PDGFR-α⁺ cells cultured under these conditions consisted of PDGFR-α⁺/Flk-1⁻ paraxial progenitors (Fig. 3F). Thus, this result suggests that the PDGFR-α⁺ population on day 6 of differentiation
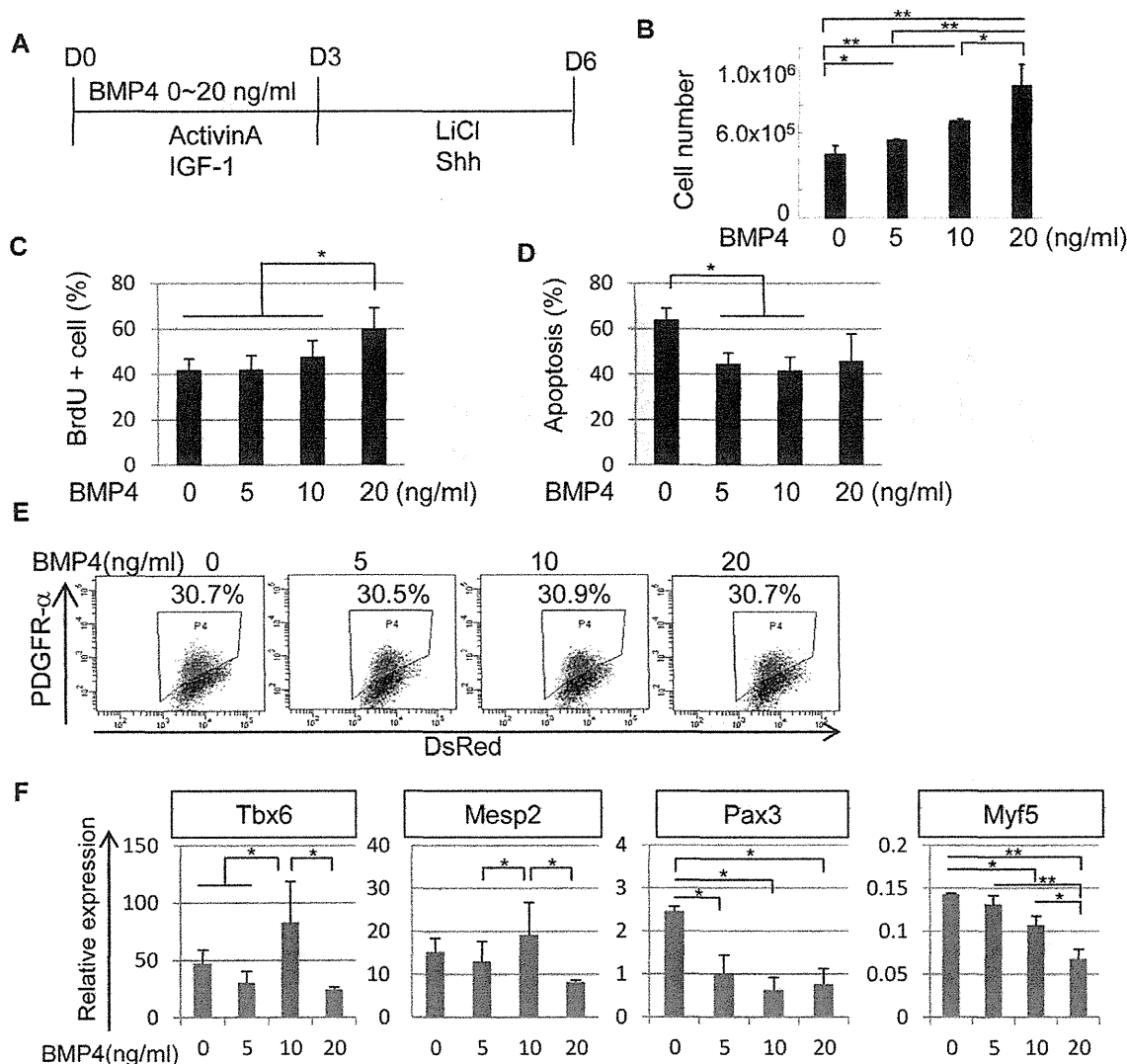
Figure 2. Effects of BMP4 on paraxial mesodermal differentiation of mouse iPS cells. (A) A scheme for the paraxial mesodermal differentiation of mouse iPS cells with different concentrations of BMP4 from D0 to D3. BMP4 was administrated from D0 to D3 at a concentration of 0–20 ng/ml. The cultures also contained Activin A (5 ng/ml), IGF-1 (10 ng/ml), LiCl (5 mM), and Shh (10 ng/ml). The cells were analyzed on D6 in (B), (E), and (F), or on day 3 (D3), as shown in (C) and (D). (B) Total number of mouse iPS cells after differentiation with the protocol shown in (A) (n = 3). (C) Proliferation of differentiated mouse iPS cells on D3 assessed by BrdU assay (n = 3). (D) Apoptosis of differentiated mouse iPS cells on D3 assessed by a proportion of PI positive/AnnexinV positive cell (n = 3). (E) The expression of PDGFR-α in mouse iPS cell differentiation culture. The percentage indicates the proportion of PDGFR-α⁺ cells (n = 3), which was not affected by BMP4. (F) Gene expression profiles of PDGFR-α⁺ cells in BMP4-induced cultures (n = 3). The expression of Tbx6 and Mesp2 was higher at a concentration of 10 ng/ml BMP4, whereas the expression of Pax3 and Myf5 was reduced at higher doses of BMP4. *p<0.05, **p<0.01 between selected two samples.
doi:10.1371/journal.pone.0047078.g002

includes mainly paraxial mesodermal progenitors rather than PDGFR-α⁺/Flk-1⁺ immature mesodermal progenitors [8].

Mouse iPS Cell-derived Paraxial Mesodermal Progenitor Cells are able to Differentiate into Myocytes, Osteocytes, and Chondrocytes in vitro

We investigated the in vitro differentiation potential of mouse iPS cell-derived PDGFR-α⁺ cells to paraxial mesoderm descendants, such as myocytes, osteocytes, and chondrocytes. PDGFR-α⁺ cells isolated by FACS Aria displayed up to 98% purity (Fig. 4A). Tbx6 positive, Mesp2 positive paraxial mesodermal cells were mainly involved in the PDGFR-α⁺ population, while Oct3/4 [28] positive,

Nanog [29,30] positive undifferentiated cells were mainly contained within the PDGFR-α⁻ population (Fig. 4B). In skeletal myogenic differentiation culture, myogenin-positive, myosin heavy chain (MHC)-positive mature myocytes were mainly detected in the PDGFR-α⁺ population, whereas very few myogenin-positive cells were derived from PDGFR-α⁻ cells (Fig. 4C). Moreover, approximately 16% of the PDGFR-α⁺ cells could give rise to myocytes, whereas only 1% of the PDGFR-α⁻ cells were myogenin positive (n = 3) (Fig. 4D). PDGFR-α⁺ cells differentiated into osteocytes containing an abundant calcium matrix, as revealed by Alizarin Red-positive staining in the well (Fig. 4E). On the other hand, the PDGFR-α⁻ population exhibited limited
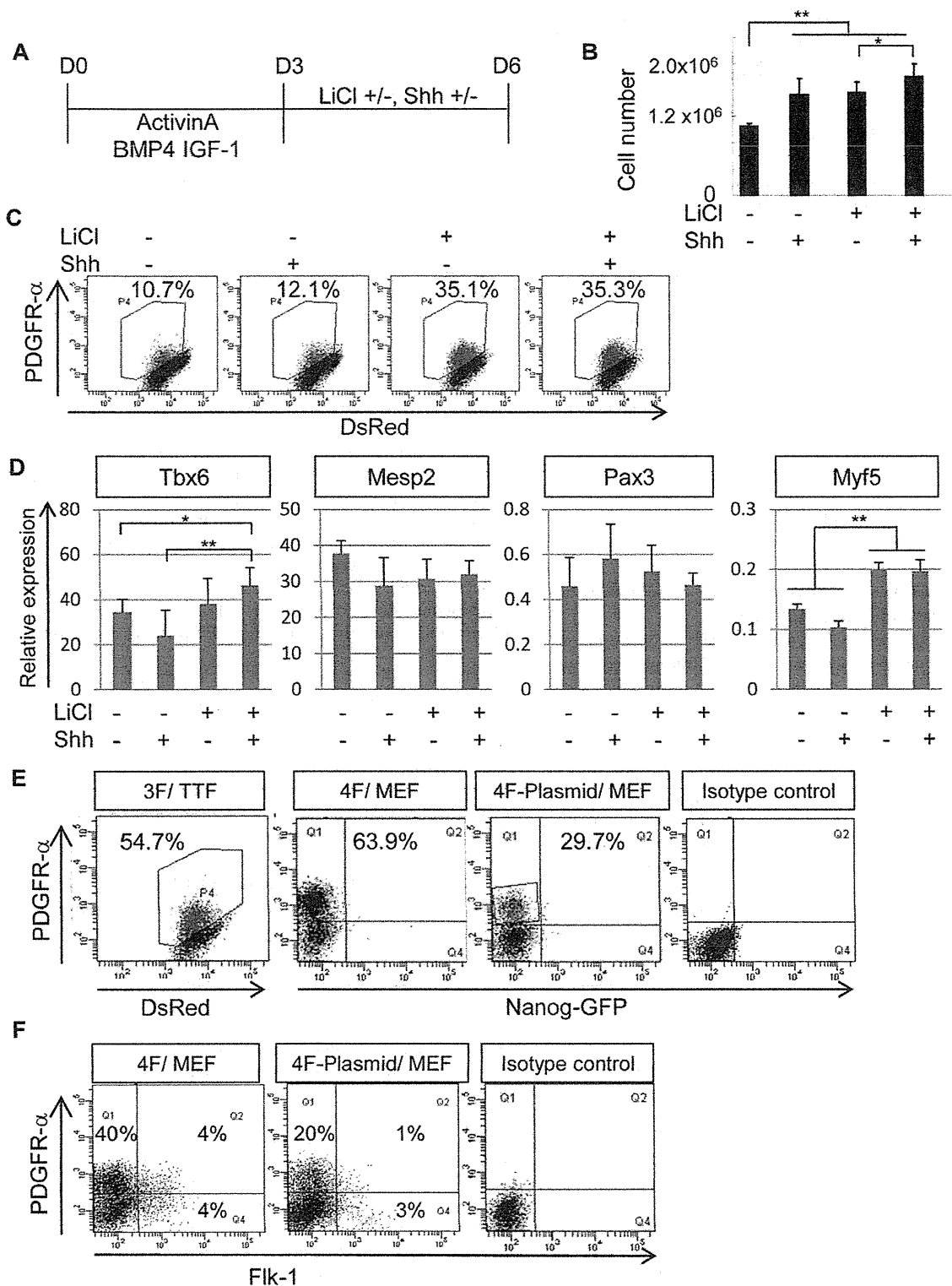
124

Figure 3. Effects of LiCl and Shh on paraxial mesodermal differentiation of mouse iPS cells. (A) A scheme for paraxial mesodermal differentiation of mouse iPS cells using various combinations of LiCl and Shh from D3 to D6. The cells were analyzed on D6 in (B–F). The cultures also contained Activin A (5 ng/ml), BMP4 (10 ng/ml), and IGF-1 (10 ng/ml). (B) Total number of mouse iPS cells after differentiation with the protocol shown in (A) (n = 3). Both LiCl and Shh enhanced proliferation of mouse iPS cells. (C) The expression of PDGFR-α in mouse iPS cells after differentiation. The percentage indicates the proportion of PDGFR-α$^+$ cells (n = 3). LiCl prominently induced generation of PDGFR-α$^+$ cells. (D) Gene expression profiles of PDGFR-α$^+$ cultured as shown in (A) (n = 3). LiCl treatment enhanced expression of *Myf-5*. (E) Differentiation of various types of

potential to form calcium-positive osteocytes, as indicated by reduced Alizarin Red staining (n = 3) (Fig. 4E). Quantification of total amount of Alizarin Red dyes in a well demonstrated that osteogenic cells were mainly contained in PDGFR-α^+ population (Fig. 4F). Furthermore, during *in vitro* chondrogenesis, the PDGFR-α^+ population formed an Alcian Blue-positive chondrocytic colony in the center of a high density micromass cell culture (Fig. 4G). In contrast, the PDGFR-α^- population did not form Alcian Blue-positive chondrocytes under the same conditions (n = 3) (Fig. 4G). Quantification of Alcian Blue-positive area in a well showed that chondrogenic cells were also contained in PDGFR-α^+ population (Fig. 4H). These results indicate that PDGFR-α^+ cells derived from mouse iPS cells had the potential to differentiate into paraxial mesodermal descendants *in vitro*, including skeletal myocytes, osteocytes, and chondrocytes. Thus, the mouse iPS cell-derived PDGFR-α^+ cells displayed paraxial mesodermal characteristics.

In vivo Differentiation Potential of Mouse iPS Cell-derived Paraxial Mesodermal Progenitor Cells

To assess the potential of PDGFR-α^+ cells to give rise to paraxial mesodermal descendants *in vivo*, we transplanted both PDGFR-α^+ and PDGFR-α^- cells (derived from DsRed/iPS cells) into the tibial anterior (TA) muscle of immunodeficient mice. Four weeks after transplantation, tumor formation was only observed in TA muscle engrafted with PDGFR-α^- cells (n = 3) (Fig. 5A). The tumor was classified as a teratoma, which consisted of all 3 germ layers (Fig. 5B, right panel) and was derived from engrafted cells that expressed DsRed (Fig. 5C, right panel). Thus, these results suggest that PDGFR-α^- cells contain undifferentiated iPS cells. Engraftment of PDGFR-α^+ cells resuspended in Matrigel caused ectopic cartilage formation in the TA muscle (n = 2 for 3 engraftments) (Fig. 5B, left panel). Ectopic cartilage was covered with a capsule and did not form part of the teratoma since it did not contain any other tissues. As shown in Fig. 5C (left panel), the ectopic cartilage was derived from engrafted cells that expressed DsRed. Transplantation into TA muscle of PDGFR-α^+ cells resuspended in Matrigel resulted in the fusion of very few DsRed-positive cells with host myofiber (data not shown), as injection with Matrigel may have caused limited migration of engrafted cells. Therefore, we performed transplantation of fractionated cells in medium. However, no iPS cell-derived cells were detected following engraftment in medium, even in the case of the PDGFR-α^- population (data not shown), which may be due to the fact that FACS-sorted cells have low adhesion potential. In order to enhance the adhesion potential of the FACS-sorted cells, PDGFR-α^+ and PDGFR-α^- cells were sorted and reseeded onto thermoresponsive culture dishes pre-coated with type IV collagen. Cells were harvested 24 h after re-culture by incubation at RT without enzymatic treatment. PDGFR-α^+ and PDGFR-α^- cells were transplanted into the TA muscle of immunodeficient mice, and the engrafted tissues were analyzed 4 weeks after transplantation (n = 3). Detection of DsRed-positive myofibers indicated that the PDGFR-α^+ cells had fused with host myofibers (Fig. 5D, white arrow). On the other hand, the PDGFR-α^- cells had never fused with myofibers and were observed in an interstitial area of

muscles (Fig. 5D, white arrowhead). DsRed expression was confirmed by using an HRP-conjugated secondary antibody to exclude autofluorescence of mouse myofibers (Fig. 5D, black arrow and black arrowhead).

To assess the contribution of the engrafted PDGFR-α^+ cells to myogenesis, we transplanted the cells into DMD-null mice, which is a model mouse for Duchenne muscular dystrophy (DMD) [31]. Four weeks after transplantation, DMD-null mice were sacrificed and dystrophin [32] expression in engrafted muscle was assessed by immunohistochemical analysis (n = 3). Dystrophin-positive myofibers were detected in TA muscle engrafted with PDGFR-α^+ cells (Fig. 5E, white arrow), while no dystrophin expression was observed in the muscle engrafted with PDGFR-α^- cells (Fig. 5E, right panel), suggesting that the PDGFR-α^+ cells have potential to differentiate into functional myogenic cells that fuse with host myofibers and produce dystrophin. The PDGFR-α^+ cells also gave rise to muscle satellite cells, which are adult stem cells of striated muscle. The expression of SM/C-2.6 (a surface marker for quiescent satellite cells [33]) and of Pax7 [34] (a specific transcriptional factor for satellite cells) was detected in some DsRed-positive engrafted cells (Fig. 5F and 5G). Therefore, to assess whether these iPS cell-derived satellite cells were functional, we isolated single cells from engrafted TA muscle by enzymatic treatment and recultured them under the culture conditions of primary satellite cells. The iPS cell-derived DsRed-positive cells were able to differentiate into MHC-positive myofibers within host myofibers together with host myocyte (Fig. 5H, white arrow). These results suggest that PDGFR-α^+ cells represent paraxial mesodermal progenitors that have the potential to differentiate into both cartilage and functional myogenic cells *in vivo*.

The Combined Use of 2 Markers–PDGFR-α and KDR–allows Isolation of Paraxial Mesodermal Progenitors from Human iPS Cell Differentiation Culture

Next, we investigated paraxial mesodermal differentiation in human iPS cells. Although we attempted to use the same differentiation protocol as for mouse iPS cells, human iPS cells were not viable under these conditions. This may be due to the inability of human pluripotent stem cells to survive as single cells. Therefore, human iPS cells were dissociated into small clusters and differentiated in defined medium containing KSR. Gene expression profile of differentiated human iPS cells was analyzed during differentiation from day 0 to day 10 (Fig. 6A). The expression of undifferentiated markers, such as *Oct3/4* [28], *Nanog* [29,30] and *Sox2* [35] gradually diminished along with differentiation (Fig. 6A). The expressions of early mesodermal marker *T* and lateral mesodermal marker *KDR* were detected after day 2 and gradually decreased as differentiation proceeded (Fig. 6A). The expression of *PDGFR-α* increased along with differentiation while paraxial mesodermal markers *Tbx6* and *Mesp2* were transiently activated at around day 4–6 (Fig.6A). Based on expression pattern of these genes, we tried to isolate paraxial mesodermal progenitors monitoring the expression of two mesodermal surface markers–PDGFR-α and KDR– at day6 differentiation. As a result, differentiated human iPS cells were separated into 4 fractions: PDGFR-α^+/KDR$^+$ (double positive; DP), PDGFR-α^+/KDR$^-$
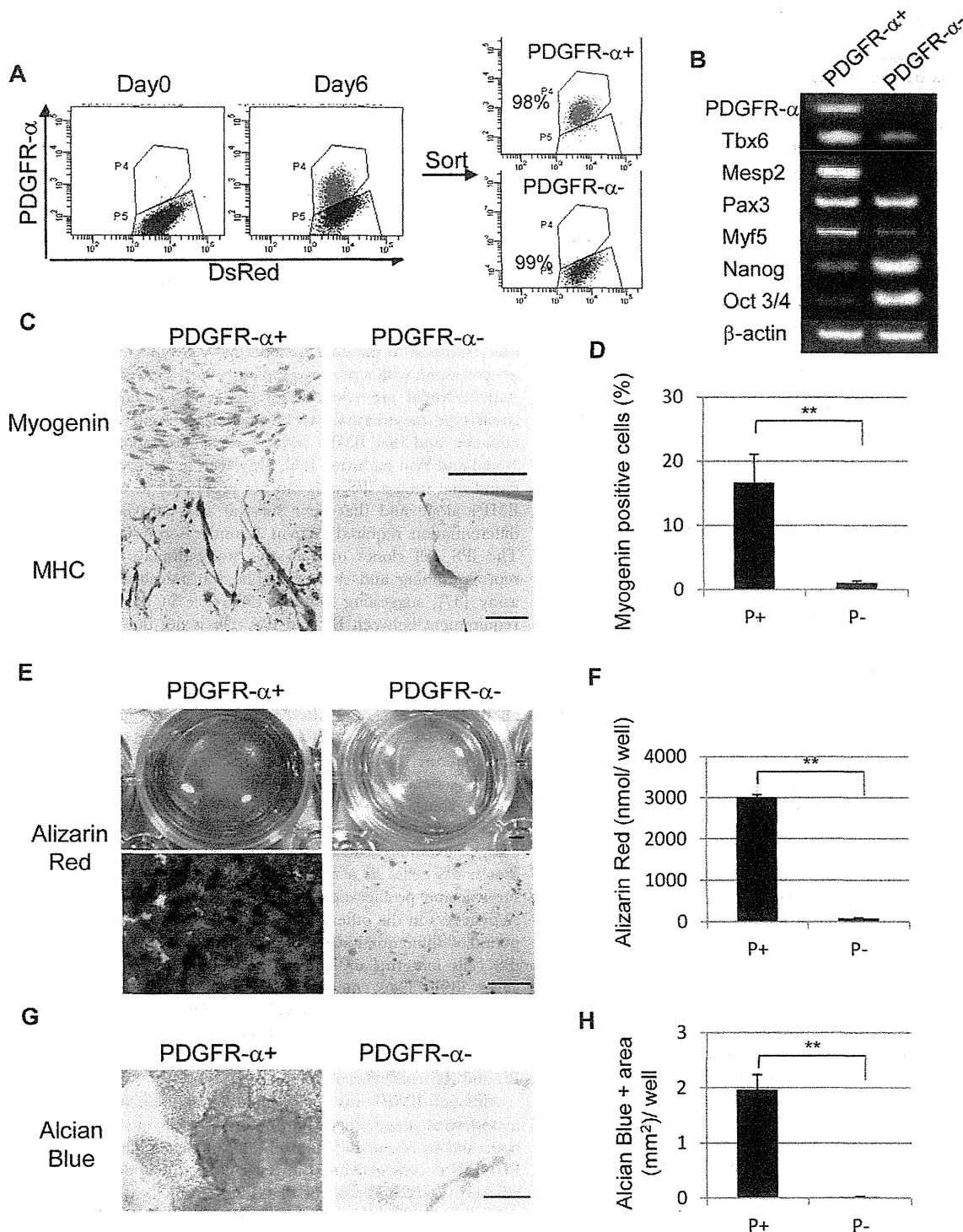
Figure 4. Differentiation potential of mouse iPS cell-derived paraxial mesodermal progenitors *in vitro.* (A) On day 6, differentiated iPS cells were sorted into PDGFR-α^+ and PDGFR-α^- populations. (B) Gene expression profile for mesodermal and undifferentiated markers in PDGFR-α^+ and PDGFR-α^- populations. (C) *In vitro* myogenic differentiation of sorted cells 7 days after differentiation. The differentiation of PDGFR-α^+ cells, but not PDGFR-α^- cells, into mature myocytes is shown as myogenin$^+$ cells with brown nuclear staining (upper panels) or as myosin heavy chain (MHC)-positive cells with brown cytosolic staining (lower panels). (D) The ratio of myogenin$^+$ cells to the total number of cells that were Giemsa-positive in each well was counted. Approximately 16% of PDGFR-α^+ cells were myogenin$^+$ (n = 3). (E) *In vitro* osteogenesis of differentiated mouse iPS cells 28 days after osteocytic induction. The PDGFR-α^+ population differentiated into osteocytes, producing an Alizarin Red-positive calcium matrix. The PDGFR-α^- population showed limited osteogenic potential, as indicated by faint calcium deposits (n = 3, each). (F) Quantification of Alizarin Red dyes in an osteogenic differentiation culture (n = 3). (G) *In vitro* chondrogenesis of differentiated mouse iPS cells 21 days after chondrocytic induction. The

127

(PDGFR-α single positive; PSP), PDGFR-α^-/KDR$^+$ (KDR single positive; KSP), and PDGFR-α^-/KDR$^-$ (double negative; DN) (Fig. 6B). As shown in Fig. 6C, the proportion of each fraction was similar in 2 distinct human iPS cell clones. Approximately one third of cells expressed PDGFR-α, and the PSP population rose to around 20% of cells in both iPS cell clones.

Previously, we reported that while the PSP population displayed paraxial mesodermal characteristics, the DP population displayed immature mesodermal characteristics during mouse ES cell differentiation [8]. Therefore, to assess the characteristics of each cell population, we performed quantitative PCR analysis of developmental markers (Fig. 6D). The expression levels of PDGFR-α and KDR were analyzed to confirm the purity of each FACs-sorted population. In both iPS cell clones, the paraxial mesodermal markers *Tbx6* and *Mesp2* were dominantly expressed in the PSP population. In contrast, the neuronal marker *Pax6* was specifically detected in the DN population, suggesting that neural lineage cells were negatively selected by the two mesodermal markers. Taken together, the gene expression profile indicates that the PSP population isolated after differentiation of human iPS cells displays paraxial mesodermal characteristics.

The PDGFR-α^+/KDR$^-$ Population Differentiated from Human iPS Cells Exhibits Paraxial Mesodermal Characteristics with Differentiating Potentials into Skeletal Myocytes, Osteocytes, and Chondrocytes *in vitro*

Next, we investigated the *in vitro* differentiation potential of the PSP population derived from human iPS cells to paraxial mesoderm descendants, such as myocytes, osteocytes, and chondrocytes. Differentiated human iPS cells at Day6 were separated into 4 fractions–DP, DN, PSP and KSP– by FACS Aria and re-cultured for further differentiation. In osteogenic differentiation culture, Alizarin Red-positive calcium matrix was dominantly detected in the culture of PSP population, indicating that PSP cells have enough potential to differentiate into osteocytes (n = 3) (Fig. 7A). Quantification of total amount of Alizarin Red dyes in a well demonstrated that osteogenic cells were mainly contained within PSP population (Fig. 7B). In chondrogenic differentiation culture, both PSP population and DP population gave rise to Alcian Blue-positive chondrocytes (n = 3) (Fig. 7C). Quantification of Alcian Blue-positive area in a well showed that chondrogenic progenitors were mainly contained in PSP population (Fig. 7D). In myogenic differentiation culture, MHC-positive mature myocytes were selectively detected in the PSP population (n = 3) (Fig. 7E and 7F). These results indicate that PSP cells derived from human iPS cells have the potential to differentiate into three paraxial mesodermal descendants *in vitro*, including skeletal myocytes, osteocytes, and chondrocytes. Thus, these results suggest that the human iPS cell-derived PSP cells represent paraxial mesodermal progenitors.

Discussion

Since Yamanaka and Takahashi first reported the generation of pluripotent ES cell-like cells–induced pluripotent stem (iPS) cells– from mouse fibroblasts by unique gene transfer-based nuclear reprogramming technology, many researchers have compared the similarities and differences between ES and iPS cells with respect to their pluripotency, undifferentiated states, genetic or epigenetic

regulations, and differentiation potentials. For lateral mesodermal differentiation into cardiomyocytes, endothelial cells, and hematopoietic cells, mouse iPS cells have almost identical differentiation potential to mouse ES cells. In the present study, we demonstrated a potential of mouse ES and iPS cells for paraxial mesodermal differentiation, with the exception of the requirement of Activin A during iPS cell differentiation under serum-free conditions.

Previously, we demonstrated that BMP4 treatment was sufficient to promote commitment of mouse ES cells to the early primitive streak-type mesodermal lineage [14] and further their differentiation to paraxial mesodermal cell types. These findings are consistent with a previous finding, which showed that Wnt and Activin/Nodal are essential for the establishment of primitive streak-type mesodermal precursors during mouse ES cell differentiation and that BMP4 induces the endogenous activation of Nodal and Wnt pathways [36]. However, in the present study, we found that mouse iPS cells did not proliferate in the presence of BMP4 alone and that their survival and paraxial mesodermal differentiation required Activin A under serum-free conditions. The iPS cell clones used in this study display near complete reprogramming and show germline transmission in a chimeric assay [37], suggesting that the difference in the growth factor requirement between ES and iPS cells is not due to incomplete reprogramming of iPS cells. We rather consider that the requirement of Activin A by iPS cells is due to their intrinsic characteristics. More than 80% of the mouse iPS cells died by apoptosis in 24 hours after serum-free differentiation without Activin A, whereas only 10% of mouse ES showed apoptosis in the same culture condition. Mouse ES cells activate endogenous Nodal/Activin signaling in an autocrine fashion to proliferate under serum-free conditions [38]. Based on the finding that mouse iPS cells express less transcripts of the Nodal gene than mouse ES cells, we examined effects of Activin A on the serum-free culture of mouse iPS cells. As a result, we attained prominently enhanced survival and proliferation of mouse iPS cells in the presence of Activin A. On the other hand, the response to Activin A in early period of differentiation was quite identical between mouse ES and iPS cells in terms of increased expression of mesoendodermal genes [39]. Thus, mouse iPS cells are likely less capable of activating Nodal/Activin signaling, which is essential for their survival rather than for differentiation. Severe conditions, such as serum-free monolayer culture, should uncover differences between ES and iPS cells efficiently.

Although BMP4 was not essential for the induction of paraxial mesodermal progenitors from mouse iPS cells in the presence of both Activin A and LiCl and did not influence the proportion of PDGFR-α^+ cells generated in cell culture, the addition of BMP4 affected the composition of PDGFR-α^+ cells in a concentration-dependent manner. In particular, 10 ng/ml of BMP4 enhanced expression of paraxial mesodermal markers, whereas higher doses of BMP4 inhibited the expression of the myogenic marker *Myf5*, as consistent with previous reports [26]. In contrast, the addition of LiCl, which activates Wnt signaling via inhibition of GSK3β, dramatically increased the proportion of PDGFR-α^+ cells in serum-free culture. Mesodermal gene expression patterns in the presence or absence of LiCl were almost identical, with the exception of elevated *Myf5* expression in the presence of LiCl. Therefore, these results suggest that Wnt signaling promotes